

# Dust-obscured star formation and AGN fuelling in hierarchical models of galaxy evolution

A. W. Blain,<sup>1,2</sup> Allon Jameson,<sup>1</sup> Ian Smail,<sup>3</sup> M. S. Longair,<sup>1</sup> J.-P. Kneib<sup>2</sup>  
and R. J. Ivison<sup>4</sup>

<sup>1</sup> *Cavendish Laboratory, Madingley Road, Cambridge, CB3 0HE, UK.*

<sup>2</sup> *Observatoire Midi-Pyrénées, 14 Avenue E. Belin, 31400 Toulouse, France.*

<sup>3</sup> *Department of Physics, University of Durham, South Road, Durham, DH1 3LE, UK.*

<sup>4</sup> *Department of Physics & Astronomy, University College London, Gower Street, London, WC1E 6BT, UK.*

12 September 2018

## ABSTRACT

A large fraction of the luminous distant submillimetre-wave galaxies recently detected using the Submillimetre Common-User Bolometer Array (SCUBA) camera on the James Clerk Maxwell Telescope appear to be associated with interacting optical counterparts. We investigate the nature of these systems using a simple hierarchical clustering model of galaxy evolution, in which the large luminosity of the SCUBA galaxies is assumed to be generated at the epoch of galaxy mergers in a burst of either star formation activity or the fuelling of an active galactic nucleus (AGN). The models are well constrained by the observed spectrum of the far-infrared/submillimetre-wave background radiation and the 60- $\mu\text{m}$  counts of low-redshift *IRAS* galaxies. The ratio between the total amount of energy released during mergers and the mass of dark matter involved must increase sharply with redshift  $z$  at  $z \lesssim 1$ , and then decrease at greater redshifts. This result is independent of the fraction of the luminosity of mergers that is produced by starbursts and AGN. One additional parameter – the reciprocal of the product of the duration of the enhanced luminosity produced by the merger and the fraction of mergers that induce an enhanced luminosity, which we call the activity parameter – is introduced, to allow the relationship between merging dark matter haloes and the observed counts of distant dusty galaxies to be investigated. The observed counts can only be reproduced if the activity parameter is greater by a factor of about 5 and 100 at redshifts of 1 and 3 respectively, as compared with the present epoch. Hence, if merging galaxies account for the population of SCUBA galaxies, then the merger process must have been much more violent at high redshifts. We discuss the counts of galaxies and the intensity of background radiation in the optical/near-infrared wavebands in the context of these hierarchical models, and thus investigate the relationship between the populations of submillimetre-selected and Lyman-break galaxies.

**Key words:** galaxies: evolution – galaxies: formation – cosmology: observations – cosmology: theory – diffuse radiation – infrared: galaxies

## 1 INTRODUCTION

The history of star formation in dusty galaxies was recently discussed by Blain et al. (1999c), who assumed that the distant galaxies recently detected using the 450/850- $\mu\text{m}$  Submillimetre Common-User Bolometer Array (SCUBA) camera (Holland et al. 1999) were the high-redshift counterparts of local ultraluminous *IRAS* galaxies. The global star for-

mation rate (SFR) in dust obscured galaxies was inferred to be significantly greater than that of optically selected high-redshift galaxies (Steidel et al. 1996a,b, 1999), subject to the uncertain fraction of the luminosity of the submillimetre-selected samples of galaxies (Smail, Ivison & Blain 1997; Barger et al. 1998; Hughes et al. 1998; Barger et al. 1999a; Blain et al. 1999b; Eales et al. 1999) that is produced by accretion processes in active galactic nuclei (AGN). A frac-

tion of at most 30 per cent, and more likely 10–20 per cent, is suggested by both follow-up observations (Frayser et al. 1998; Ivison et al. 1998; Smail et al. 1998; Barger et al. 1999b; Frayer et al. 1999; Lilly et al. 1999), and information derived in other wavebands; see section 5.4 of Blain et al. (1999c), Almaini, Lawrence & Boyle (1999) and Gunn & Shanks (1999). Using a different approach, in which the high-redshift SCUBA population is decoupled from the local infrared-luminous galaxies, Trentham, Blain & Goldader (1999) were able to reconcile the SCUBA counts with a less dramatic amount of obscured star-formation activity. Use another empirical approach, Tan, Silk & Balland (1999) derived results somewhere between the two. A summary of the existing data on the history of star formation is presented in Fig. 1.

Although well constrained, and in accord with the available observational data, the models in Blain et al. (1999c) and Trentham et al. (1999) included few details of the physical origin of the large luminosity of SCUBA galaxies. Semi-analytic models of hierarchical galaxy formation, in which galaxies assemble by the merger of progressively larger subunits (Cole et al. 1994; Baugh et al. 1998; Kauffmann & Charlot 1998; Somerville, Primack & Faber 1999) have been used to account for a wide range of observations in the optical and near-infrared wavebands, and have been extended into the far-infrared and submillimetre wavebands by Guiderdoni et al. (1998). These models involve a large number of free parameters, and the interplay between them can make it difficult to identify the most important physics responsible for a particular observation. In this paper we develop a model of infrared-luminous galaxies in a simple version of such a scenario (Blain & Longair 1993a,b; Jameson, Longair & Blain 1999), which includes many fewer parameters and hopefully makes the astrophysics more transparent. We attempt to reproduce the SCUBA counts by invoking bright dust-enshrouded bursts of either star formation activity or AGN fuelling at the epochs of mergers.

Motivation for considering the SCUBA galaxies as luminous mergers is provided by both the optical identifications of the Smail et al. (1998) sample, which appear to contain a large fraction of interacting galaxies, and the gas consumption rate that is inferred from observations of CO emission of two submillimetre-selected galaxies made using the Owens Valley Millimeter Array (Frayser et al. 1998, 1999), which cannot be sustained for more than a few  $10^8$  yr. Even the faint and compact counterparts listed in Smail et al. (1998) could be merging galaxies, but too faint to identify as such; see the simulations of the appearance of high-redshift mergers in Bekki, Shioya & Tanaka (1999). If the SCUBA galaxies are the high-redshift counterparts of the low-redshift ultra-luminous infrared galaxies, which are predominantly merging systems, then this also offers support for modeling the SCUBA galaxies as mergers. Using our simple model, we emphasise the most important features and the underlying physics of the evolution of submillimetre-selected galaxies and their relationship to the population of quiescent galaxies.

In Section 2 we describe the details of the model, and investigate the constraints imposed by the intensity of the far-infrared and submillimetre-wave background radiation and the counts of low-redshift *IRAS* galaxies. We discuss the evolution of the luminosity density in the model and

compare the models with observations in the same way as the evolving *IRAS* luminosity function models discussed by Blain et al. (1999c). In Section 3 we discuss the predictions in the context of source counts in the submillimetre and far-infrared wavebands, and investigate whether the SCUBA galaxies can easily be explained in an hierarchical picture of galaxy formation and evolution. In Section 4 the corresponding background radiation intensities and galaxy counts in the near-infrared and optical wavebands are discussed. In Section 5 we review the parameters we have introduced to describe the models. We present our main conclusions in Section 6. A value of Hubble's constant  $H_0 = 100h \text{ km s}^{-1} \text{ Mpc}^{-1}$ , with  $h = 0.5$ , a density parameter  $\Omega_0 = 1$  and a cosmological constant  $\Omega_\Lambda = 0$  are assumed.

## 2 AN ANALYTIC HIERARCHICAL PICTURE

The evolution of galaxy-scale structures under gravity according to hierarchical clustering models can be analysed using the Press–Schechter formalism (Press & Schechter 1974), which describes the time-dependent mass spectrum of bound objects. The analytic results of the Press–Schechter formalism are in quite acceptable agreement with those of N-body simulations (Brainerd & Villumsen 1992). The formalism can be extended to yield a very straightforward semi-analytic merger rate, under the single assumption that the process of halo mergers is independent of mass (Blain & Longair 1993a,b).

### 2.1 The Press–Schechter Formalism

According to the Press–Schechter prescription, the mass spectrum of bound objects with masses between  $M$  and  $M + dM$  is

$$N_{\text{PS}}(M, z) = \frac{\bar{\rho}}{\sqrt{\pi}} \frac{\gamma}{M^2} \left( \frac{M}{M^*} \right)^{\gamma/2} \exp \left[ - \left( \frac{M}{M^*} \right)^\gamma \right], \quad (1)$$

in which  $\bar{\rho}$  is the smoothed comoving density of the Universe, dominated by dark matter,  $\gamma = (3 + n)/3$ , where  $n$  is the power-law index of primordial density fluctuations, and  $M^*(z)$  is a parameter which describes the evolution of density fluctuations as a function of redshift  $z$ :

$$M^*(z) = M^*(0) \left[ \frac{\delta(z)}{\delta(0)} \right]^{2/\gamma}. \quad (2)$$

$\delta(z)$  is the function describing the growth of perturbations in a general cosmology, and is derived from the equation,

$$\ddot{\delta} + 2 \frac{\dot{R}}{R} \dot{\delta} - \frac{4\pi G \bar{\rho}}{R^3} \delta = 0, \quad (3)$$

in which  $R$  is the scalefactor of the Universe. In an Einstein de-Sitter model, the growing mode has  $\delta \propto (1 + z)^{-1}$ .  $M^*(0)$  is the typical mass of bound objects at  $z = 0$ . Inhomogeneities do not grow if  $\gamma \leq 0$ , that is if  $n \leq -3$ . For scale-invariant density fluctuations,  $n = 1$  or  $\gamma = 4/3$ . This is close to the value observed on the largest scales from the cosmic microwave background radiation (CMBR). Observations of large-scale structure indicate that  $n \simeq -1.5$ , or  $\gamma \simeq 1/2$ , on the smallest scales (Peacock & Dodds 1994), which can be associated with the transfer function between

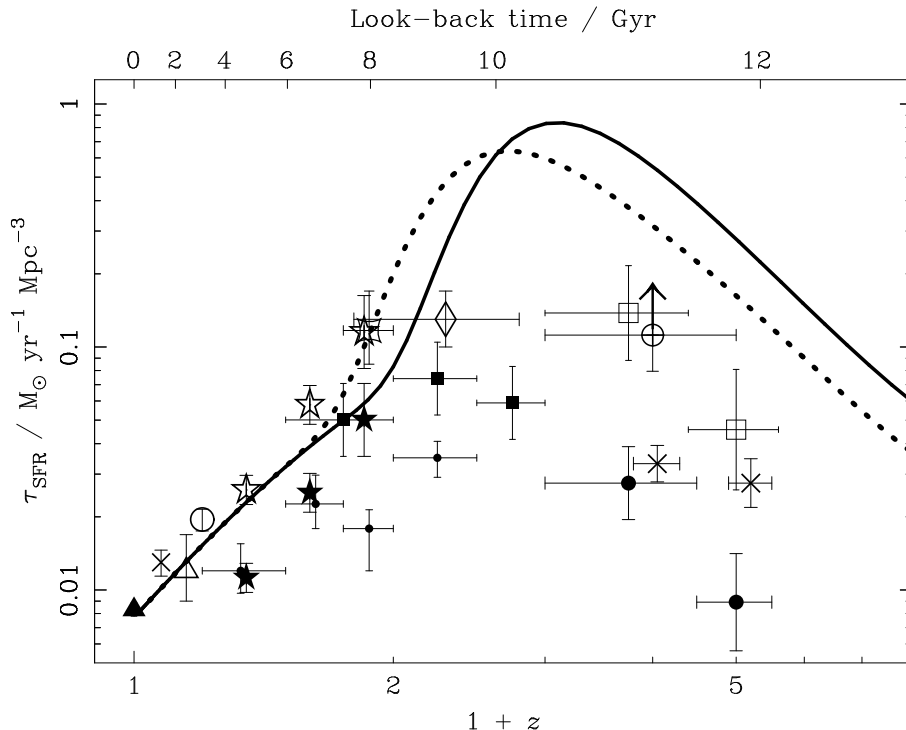


**Figure 1.** The SFR as a function of redshift,  $\tau_{\text{SFR}}(z)$ , as inferred from ultraviolet/optical/near-infrared observations, in order of increasing redshift, by Gallego et al. (1996; filled triangle), Gronwall (1999; thin diagonal cross), Treyer et al. (1998; open triangle), Tresse & Maddox (1998; empty circle), Lilly et al. (1996; filled stars), Cowie, Songaila & Barger (1999; small filled circles); Glazebrook et al. (1999; bent square at  $z = 0.9$ ), Connolly et al. (1997; filled squares), Yan et al. (1999; empty lozenge), Madau et al. (1996; large filled circles), and Pettini et al. (1998a,b; empty squares). Flores et al. (1999; empty stars) and Pettini et al. (1998a,b) have corrected the Lilly et al. and Madau et al. results respectively for observed dust extinction. The high-redshift points are derived from analyses of the *Hubble Deep Field (HDF)*. A recent ground-based survey of a wider area by Steidel et al. (1999) increased the estimated high-redshift SFR, as shown by the thick diagonal crosses. No extinction correction is applied to these points; Steidel et al. (1999) estimate that the extinction-corrected SFR is greater by a factor of about 5. Other analyses of the *HDF* data by Sawicki, Lin & Yee (1997) and Pascarella, Lanzetta & Fernández-Soto (1998) yielded similar results. Cowie, Songaila & Barger (1999) have argued recently that the low-redshift SFR increases more gradually, as  $(1+z)^\gamma$  with  $\gamma \simeq 1.5$ , in contrast with the usual  $\gamma \simeq 4$  (Lilly et al. 1996). At longer wavelengths, SFRs have been derived from mid-infrared observations by Flores et al. (1999) and from submillimetre-wave observations by Blain et al. (1999c; lines) and Hughes et al. (1998; empty circle with upward pointing arrow). Cram (1998) investigated the star-formation history at  $z \lesssim 1$  using radio observations, deriving a rate of  $2.5 \times 10^{-2} M_{\odot} \text{ yr}^{-1} \text{ Mpc}^{-3}$  at  $z = 0$ , which increases by an order of magnitude at  $z \simeq 1$ . The submillimetre-based Gaussian and modified Gaussian SFR models (see Blain et al. 1999c and Barger et al. 1999b) are represented by the solid and dotted lines respectively. A better fit to the preliminary redshift distribution of submillimetre-selected galaxies (Barger et al. 1999b) is provided by the modified model, in which the parameters  $H$ ,  $\sigma$  and  $z_p$  (Blain et al. 1999c) take the values 70, 1 Gyr and 1.7 respectively, as compared with 95, 0.8 Gyr and 2.1 in the original model. The total amount of star formation/AGN fuelling activity taking place in the modified Gaussian model is 90 per cent of that in the original Gaussian model.

a primordial  $n = 1$  spectrum and the spectrum after recombination.

Using the Tully–Fisher relation (Hudson et al. 1998), Blain, Möller & Maller (1999) obtained a value  $M^*(0) = 3.6 \times 10^{12} M_{\odot}$ . The exact value of  $M^*(0)$  is not very important here, as a mass-to-light ratio is introduced to convert the mass spectrum into a luminosity function.

## 2.2 Deriving a merger rate

Working from the mass spectrum  $N_{\text{PS}}(M, z)$ , Blain & Longair (1993a,b) showed that a formation rate of bound objects  $\dot{N}_{\text{form}}(M, z)$  in galaxy halo mergers can be constructed if the mass distribution of the components involved in a statistical sample of merger events is assumed to be independent

of mass. In this case, the merger rate can be represented accurately by the function

$$\dot{N}_{\text{form}} = \dot{N}_{\text{PS}} + \phi \frac{\dot{M}^*}{M^*} N_{\text{PS}} \exp \left[ (1 - \alpha) \left( \frac{M}{M^*} \right)^\gamma \right], \quad (4)$$

where

$$\dot{N}_{\text{PS}} = \gamma \frac{\dot{M}^*}{M^*} N_{\text{PS}} \left[ \left( \frac{M}{M^*} \right)^\gamma - \frac{1}{2} \right]. \quad (5)$$

$\phi$  and  $\alpha$  are numerical constants, typically about 1.7 and 1.4; their exact values depend on the assumed mass distribution of merging components (Blain & Longair 1993a), but have little effect on the results. The values of both  $\phi$  and  $\alpha$  are weak functions of  $\gamma$  and depend on the world model parameters, but the form  $\phi/\sqrt{\alpha}$  that appears in the calculations of the background radiation intensity and metal abundance is almost independent of the value of  $\gamma$ .

### 2.3 Deriving observable quantities

The merger rate as a function of mass  $\dot{N}_{\text{form}}$  can be readily used to estimate a number of observable quantities, starting with the luminosity density (or volume emissivity),

$$\epsilon_{\text{L}}(z) = 0.007c^2 \frac{x(z)}{1 - f_{\text{A}}} \int M \dot{N}_{\text{form}} dM, \quad (6)$$

in which  $x(z)$  is the ratio of the mass of baryonic matter converted into metals by nucleosynthesis in a merger-induced starburst to the total dark mass involved in the merger. The rationale behind this form of relation is given by Longair (1998). The factor of 0.007 is the approximate efficiency of conversion of mass into energy in stellar nucleosynthesis. The parameter  $f_{\text{A}} < 1$  describes the fraction of the total luminosity of merging galaxies that is attributable to accretion in AGN, and is expected to lie in the range  $0.1 \leq f_{\text{A}} \leq 0.3$  (Genzel et al. 1998; Lutz et al. 1998; Almaini et al. 1999; Barger et al. 1999b; Gunn & Shanks 1999). The parameter  $x(z)$  is expected to vary with redshift  $z$ . Blain & Longair (1993b) predicted a flat background spectrum in the sub-millimetre and far-infrared wavebands, assuming a constant value of  $x$ . Subsequent observations (e.g. Fixsen et al. 1998) demand a redshift-dependent form of  $x(z)$ , as discussed by Blain et al. (1999c).

By evaluating the integral in equation (6), the luminosity density can be expressed as

$$\epsilon_{\text{L}}(z) = 0.007c^2 \frac{x(z)}{1 - f_{\text{A}}} \bar{\rho} \frac{\phi}{\sqrt{\alpha}} \frac{\dot{M}^*}{M^*}. \quad (7)$$

Interestingly,

$$\frac{\dot{M}^*}{M^*} = \frac{2}{\gamma} \frac{\delta(z)}{\delta(z)}, \quad (8)$$

and so, because the density contrast  $\delta(z)$  is not a function of the perturbation spectral index  $\gamma$ , the  $\gamma$  dependence in this term is just a simple scaling. Thus the effect of the value of  $\gamma$  on the background radiation intensity can be studied or removed very easily. In an Einstein–de Sitter model the luminosity density  $\epsilon_{\text{L}} \propto x(z)(1+z)^{3/2}$ .

The comoving density of metals produced in starbursts between a redshift  $z_0$ , at which star formation activity begins, and  $z$ , is

$$\rho_{\text{m}}(z) = \bar{\rho} \frac{\phi}{\sqrt{\alpha}} \int_z^{z_0} \frac{1}{c} \frac{x(z)}{(1+z)} \frac{\dot{M}^*}{M^*} \frac{dr}{dz} dz, \quad (9)$$

where  $r$  is the radial comoving distance coordinate. Note that this result depends on the merger efficiency parameter  $x$  but not on the AGN fraction  $f_{\text{A}}$ , as metals are only generated in merger-induced starbursts and not in AGN fuelling events. Similarly, the background radiation intensity per unit solid angle emitted by these galaxies, which have a spectral energy distribution (SED)  $f_{\nu}$ , is

$$I_{\nu} = \frac{1}{4\pi} \int_0^{z_0} \frac{\epsilon_{\text{L}}(z)}{1+z} \frac{f_{\nu(1+z)}}{\int f_{\nu'} d\nu'} \frac{dr}{dz} dz. \quad (10)$$

If the form of  $\epsilon_{\text{L}}$  (equation 7) is included explicitly, then

$$I_{\nu} = \frac{0.007c^2 \bar{\rho}}{4\pi(1 - f_{\text{A}})} \frac{\phi}{\sqrt{\alpha}} \int_0^{z_0} \frac{x(z)}{1+z} \frac{\dot{M}^*}{M^*} \frac{f_{\nu(1+z)}}{\int f_{\nu'} d\nu'} \frac{dr}{dz} dz. \quad (11)$$

Details of the assumed dust SED can be found in Blain et al. (1999c). The mid-infrared SED is assumed to take the form  $f_{\nu} \propto \nu^{-1.7}$ .

None of the quantities listed above are affected by the time dependence of the release of energy during merging events; however, the source count requires the time profile of the merger induced starburst/AGN to be included. For simplicity, this profile is assumed to have a top-hat form with duration  $\sigma$ . The time profile of the luminosity generated in a detailed simulation of the merger of gas-rich galaxies is discussed by Mihos & Hernquist (1996), Bekki et al. (1999) and Mihos (1999). The typical duration of AGN fuelling events and starbursts may differ; for example, a lower limit to the duration of a starburst is set by the lifetime of the highest mass stars, but there is no lower limit to the duration of an AGN fuelling event. However, to avoid introducing an unnecessarily complicated model, the time-scale of a merger induced luminous phase is assumed to be independent of its origin. In addition, because not all the mergers of dark matter haloes that take place at each epoch need induce a starburst/AGN, a fraction  $F \leq 1$  is assumed. Again, this fraction could differ for starbursts and AGN, but for simplicity it is assumed not to. The luminosity of a typical merger induced starburst/AGN of mass  $M$  is thus

$$L(M, z) = 0.007c^2 \frac{x(z)}{1 - f_{\text{A}}} \frac{1}{F\sigma} M. \quad (12)$$

The source count  $N$  of galaxies per unit solid angle brighter than a flux density  $S_{\nu}$  is

$$N(S_{\nu}) = \int_0^{z_0} \int_{M_{\text{min}}}^{\infty} F\sigma \dot{N}_{\text{form}}(M, z) dM D^2(z) \frac{dr}{dz} dz, \quad (13)$$

where  $D(z)$  is the comoving distance parameter. The minimum mass merger visible at a flux density  $S_{\nu}$  and redshift  $z$  is

$$M_{\text{min}} = \frac{4\pi D^2(1+z)S_{\nu}}{0.007c^2} \frac{F\sigma}{x(z)} (1 - f_{\text{A}}) \frac{\int f_{\nu'} d\nu'}{f_{\nu(1+z)}}. \quad (14)$$

The time-scale and bursting fraction parameters,  $\sigma$  and  $F$ , always appear together in calculations, and thus the single parameter  $F\sigma$  is constrained by observations. We define  $(F\sigma)^{-1}$  to be the activity parameter, which is large in violent starbursts/AGN and free to vary as a function of redshift. The rate of energy release within each individual starburst/AGN is controlled by the value of the activity parameter. Within a representative cosmological volume the presence of a population of either rare long-lived or common short-lived starbursts/AGN cannot be distinguished. This is why the time-scale and bursting fraction parameters  $\sigma$  and  $F$  are bound together in the activity parameter.

Incorporating redshift evolution of the activity parameter introduces another degree of freedom into the count model, in addition to that provided by the redshift evolution of the star formation/AGN fuelling efficiency parameter  $x$ . Of course,  $x$ ,  $F$  and the time-scale  $\sigma$  are also free to vary as a function of mass. At present, we find no compelling reason to incorporate this additional complication into the model.

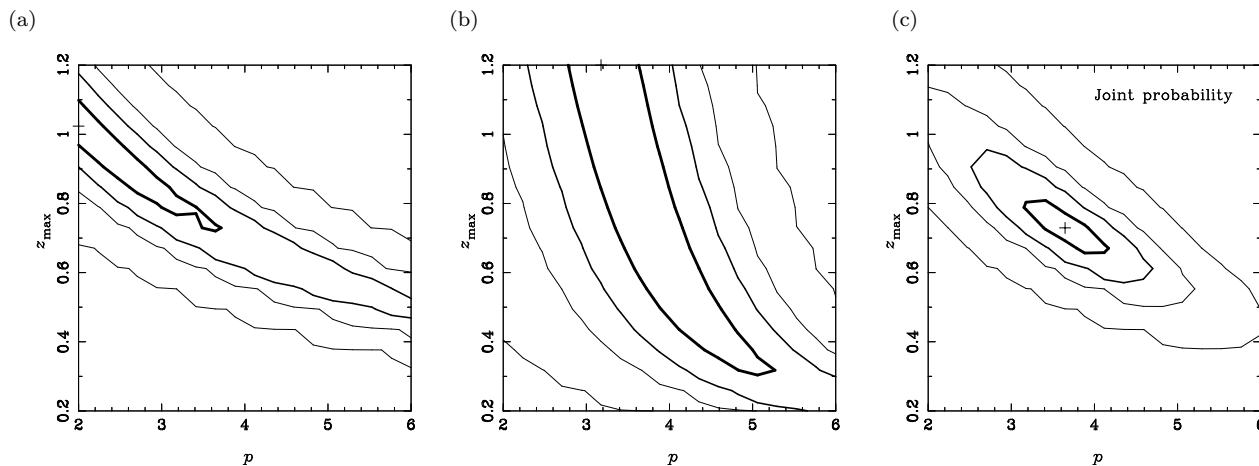


**Figure 2.** The results of fitting (a) the background radiation spectrum, (b) the shape of the *IRAS* 60- $\mu\text{m}$  counts (see Fig. 4a for references to the data) and (c) both sets of data. The contours are drawn 1, 2, 3 and  $5\sigma$  away from the peak probability, which is marked by a cross. This example is calculated for  $T_d = 45$  K.

**Table 1.** Values of the parameters  $p$  and  $z_{\text{max}}$  required in the expression for the merger efficiency  $x(z)$  (equation 16) to fit the submillimetre/far-infrared background radiation spectrum and the low-redshift 60- $\mu\text{m}$  *IRAS* galaxy counts as a function of assumed dust temperature  $T_d$ . The corresponding values of  $x_0$ ,  $F\sigma$  and  $\Omega_m$  are also listed.  $F \leq 1$ . The star formation histories associated with these models are shown in Fig. 7. Note that the most intense star formation activity takes place at a redshift  $z \simeq 5z_{\text{max}}$ .

$T_d/\text{K}$	$p$	$z_{\text{max}}$	$x_0/\gamma(1-f_A)$	$(F\sigma/\gamma)/\text{Gyr}$ (at $z=0$ )	$\Omega_m/10^{-3}$ $\times(1-f_A)$
35	4.4	0.44	$4.32 \times 10^{-5}$	0.040	1.2
40	4.0	0.55	$4.08 \times 10^{-5}$	0.041	1.3
45	3.3	0.73	$4.68 \times 10^{-5}$	0.063	1.4
50	2.7	0.96	$6.36 \times 10^{-5}$	0.141	1.7

## 2.4 Constraining the parameters

The background radiation intensities and source counts calculated from the equations derived above depend on a range of parameters: the world model, defined by  $H_0$ ,  $\Omega_0$  and  $\Omega_\Lambda$ ; the perturbation spectral index  $n$  and the value of  $M^*(0)$ ; the constants  $\phi$  and  $\alpha$  in the merger rate; the merger efficiency  $x(z)$ ; the AGN fraction  $f_A$ ; the fraction of mergers that lead to a starburst/AGN  $F$ ; their duration  $\sigma$ ; and their SED  $f_\nu$ .

Blain et al. (1999c) used the low-redshift 60- $\mu\text{m}$  *IRAS* source count and the 175- $\mu\text{m}$  *ISO* counts to constrain their models; here, however, we use the bright 60- $\mu\text{m}$  counts and the form of the far-infrared/submillimetre background spectrum, the two best determined observables, to constrain the parameters that describe the merger efficiency  $x(z)$ . If the SED does not depend on the mass of the merging galaxies, then the background spectrum (equation 10) is determined entirely by the form of the merger efficiency  $x(z)$ ,

$$I_\nu \propto \frac{\phi}{\gamma\sqrt{\alpha}} \int_0^{z_0} \frac{x(z)}{1-f_A} \frac{\dot{\delta}(z)}{\delta(z)} \frac{1}{1+z} \frac{f_\nu(1+z)}{f_{\nu'}} \frac{dr}{dz} dz. \quad (15)$$

Note that the dependence of  $I_\nu$  on the perturbation index

$n$  through  $\gamma$  is completely separate from the dependence on the world model. Thus the background spectrum determined by Puget et al. (1996), Guiderdoni et al. (1997), Dwek et al. (1998), Fixsen et al. (1998), Hauser et al. (1998), Schlegel, Finkbeiner & Davis (1998) and Lagache et al. (1999) can always be used to constrain the form of the merger efficiency  $x(z)$ . We adopt a form of  $x(z)$  identical to the ‘peak model’ described in Blain et al. (1999c): \*

$$x(z) = 2x_0 \left[ 1 + \exp \frac{z}{z_{\text{max}}} \right]^{-1} (1+z)^{p+(2z_{\text{max}})^{-1}}. \quad (16)$$

This is not a uniquely appropriate functional form of  $x(z)$ . It was originally chosen to allow the star-formation history derived by Madau et al. (1996) to be fitted. Its three parameters can be manipulated to produce a wide range of plausible star formation histories. The three parameters are:  $p$ , the asymptotic low-redshift slope of the merger efficiency  $x(z)$  in  $(1+z)$ ;  $z_{\text{max}}$ , the redshift above which the high-redshift exponential cut-off starts to take effect; and  $x_0$  the value of  $x(0)$ . The epoch of most intense star-formation/AGN-fuelling corresponds to a redshift  $z \simeq 5z_{\text{max}}$  in these models.

In Figs 2(a) and (b) the probabilities of fitting the background radiation spectrum and the slope of the 60- $\mu\text{m}$  counts predicted from the merger efficiency  $x(z)$ , defined in equation (16), to observations are shown as a function of the key parameters  $p$  and  $z_{\text{max}}$ , as an example for a dust temperature of 45 K. In Fig. 2(c) the joint probability of fitting both sets of data is shown. Note that a constant dust temperature is assumed. The value of  $f_A$  does not affect the results. If different dust temperatures are assumed, then the position of maximum probability moves around the  $p$ - $z_{\text{max}}$  plane. However, when the form of the evolution of luminosity density is calculated for each temperature, the curve has a similar form. The best-fitting values of  $p$  and  $z_{\text{max}}$ , and the corresponding values of the merger efficiency  $x_0$ , the activity parameter  $(F\sigma)_0^{-1}$  and the density parameter in metals at  $z=0$ ,  $\Omega_m$ , are presented in Table 1 for four plausible values of the dust temperature: 35, 40, 45 and 50 K. Note that the

\* Note that the form of this equation published in Blain et al. (1999c) contained a typographical error in the index of  $(1+z)$ .

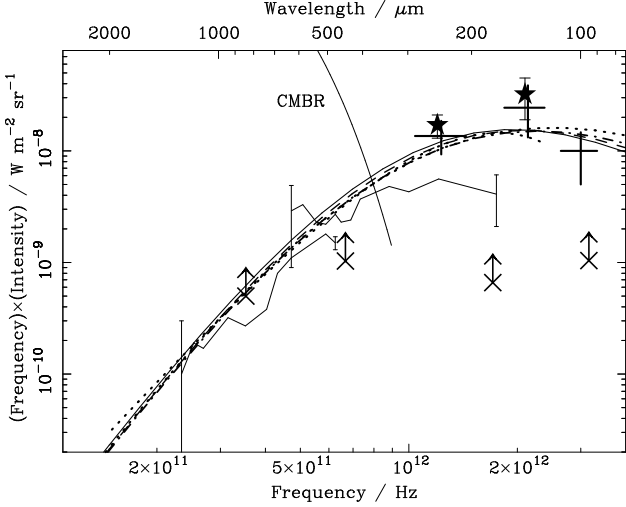


**Figure 3.** The intensity of background radiation in the millimetre, submillimetre and far-infrared wavebands, as deduced by: Puget et al. (1996) – thin solid lines with error bars at the ends; Fixsen et al. (1998) – thin dotted line that ends within the frame; Schlegel et al. (1998) – stars; Hauser et al. (1998) and Dwek et al. (1998) – thick solid crosses. The diagonal crosses represent lower limits to the background intensity inferred from source counts. From left to right: the 850- $\mu\text{m}$  count of Blain et al. (1999b); the 450- $\mu\text{m}$  count of Smail et al. (1997), as updated to include more recent information from Ivison et al. (1999); and the 175- and 95- $\mu\text{m}$  counts of Kawara et al. (1998) and Puget et al. (1999). The background spectrum predicted in the 35-, 40-, 45- and 50-K models (Table 1) are represented by solid, dashed, dot-dashed and dotted lines respectively, and are plotted across the entire abscissa. In a recent paper, Lagache et al. (1999) claim to have detected a warm diffuse Galactic dust component that accounts for about 50 per cent of the isotropic DIRBE signal attributed to the extragalactic background intensity by Hauser et al. (1998) and Schlegel et al. (1998).

best fitting values of  $p$  and  $z_{\text{max}}$  depend only weakly on the world model assumed.

The physical processes that demand a form of luminosity density which rises steeply with increasing redshift before turning over have not been considered here in any detail. It seems likely, however, that the steep decline in the star formation rate to the present day is related to the declining gas content of galaxies at  $z \lesssim 1$ , and that the behaviour at high redshifts could be attributable to relatively inefficient cooling of gas and thus of star formation in the mergers of metal-poor high-redshift systems (see Pei & Fall 1995 and Pei, Fall & Hauser 1999 for discussions of gas and dust evolution in the Universe). We discuss these issues further in Jameson, Blain & Longair (2000).

The bright low-redshift 60- $\mu\text{m}$  count,

$$N_{60} \propto \sqrt{\frac{x_0^3}{(F\sigma)_0(1-f_A)^3}} S_{60}^{-3/2}, \quad (17)$$

is independent of the cosmological model. At  $S_{60} = 10$  Jy,  $N_{60} = 19 \pm 2 \text{ sr}^{-1}$  (Saunders et al. 1990). A value of  $\sqrt{x_0^3/(F\sigma)_0(1-f_A)^3} = (11 \pm 2)\gamma \times 10^{-7} \text{ Gyr}^{-1/2}$  provides a good fit for any dust temperature between 30 and 60 K. The values of the normalization of the luminosity density  $x_0/(1-f_A)$  and the activity parameter  $(F\sigma)_0^{-1}$  at  $z \simeq 0$

that are required to fit the background spectrum and 60- $\mu\text{m}$  counts depend on the fluctuation index  $\gamma$  as  $\gamma^{-1}$  and  $\gamma$  respectively. Thus the mass-to-light ratio of merging galaxies (equation 12) is expected to be independent of the value of the perturbation index. The values of  $F\sigma$  listed in Table 1 are lower limits to the time-scale of the starburst/AGN  $\sigma$ , as  $F \leq 1$ . They are generally consistent with the starburst time-scales of order  $5 \times 10^7$  yr derived by Mihos & Hernquist (1996) from hydrodynamical simulations of galaxy mergers.

The background radiation spectra and 60- $\mu\text{m}$  counts corresponding to the models listed in Table 1 are shown in Figs 3 and 4(a) respectively. Note that the inclusion of positive evolution in the efficiency parameter  $x(z)$  overcomes the underprediction of the 60- $\mu\text{m}$  counts in the constant- $x$  model of Blain & Longair (1996); see their fig. 6. The slope of the 60- $\mu\text{m}$  counts in the new model also more adequately represents the data than the predictions of Guiderdoni et al. (1998). The luminosity function of nearby dusty galaxies at 60- $\mu\text{m}$  (Saunders et al. 1990; Soifer & Neugebauer 1991) predicted in the 40-K model, which is calculated at  $z = 0$  by evaluating  $F\sigma\dot{N}_{\text{form}}$  at the mass corresponding to a luminosity  $L$  in equation (12), is shown in Fig. 4(b). The form of the luminosity function depends on the value of the perturbation index  $\gamma$ , even though the 60- $\mu\text{m}$  counts are independent of  $\gamma$ . The best representation of the observed function is provided by a value of  $\gamma = 2/3$ , or  $n \simeq -1$ . A similar high-luminosity slope could be achieved by modifying the form of equation (12) so that  $L \propto M^\beta$ , where  $\beta > 1$ . However, to match the observations with a scale-independent value of  $n = 1$ , a rather extreme value of  $\beta = 2$  is required. In the work that follows  $n$  is assumed to take the value  $-1$ , similar to the value found for this range of masses by Peacock & Dodds (1994). In this case, the faint-end slope of the low-redshift 60- $\mu\text{m}$  luminosity function is equivalent to a Schechter function parameter  $\alpha = -5/3$  (Schechter 1976). This is the same as the faint-end slope  $\alpha = -1.60 \pm 0.13$  of the optically selected luminosity function derived by Steidel et al. (1999) at  $z \simeq 3$ , which describes the most numerous population of high-redshift galaxies that are actively forming stars. At  $0.75 < z < 1$ , the luminosity function of the blue star-forming galaxies in the CFRS survey also has a faint end slope  $\alpha = -1.56$  (Lilly et al. 1995). Steep faint-end slopes with indices of about  $-1.8$  are expected for the luminosity functions of dwarf, irregular and infrared-luminous galaxies, as discussed by Hogg & Phinney (1997).

## 2.5 Self-consistency

In section 4 of Blain et al. (1999c) the self-consistency of models of dust-obscured galaxy formation was discussed. We demanded that a sufficiently large mass of metals, and associated dust, was required to be generated by nucleosynthesis at each epoch to account for the far-infrared emission predicted by the model. As the mass of dust required to generate a given far-infrared luminosity depends strongly on the dust temperature, this consistency condition is most easily expressed as a minimum dust temperature at each redshift. In the cases of the models listed in Table 1, this lower limit to the dust temperature is presented in Fig. 5, both with and without an assumed high-redshift Population III to generate dust. If 2 per cent of the total star formation activity takes place in a high-redshift Population III, then

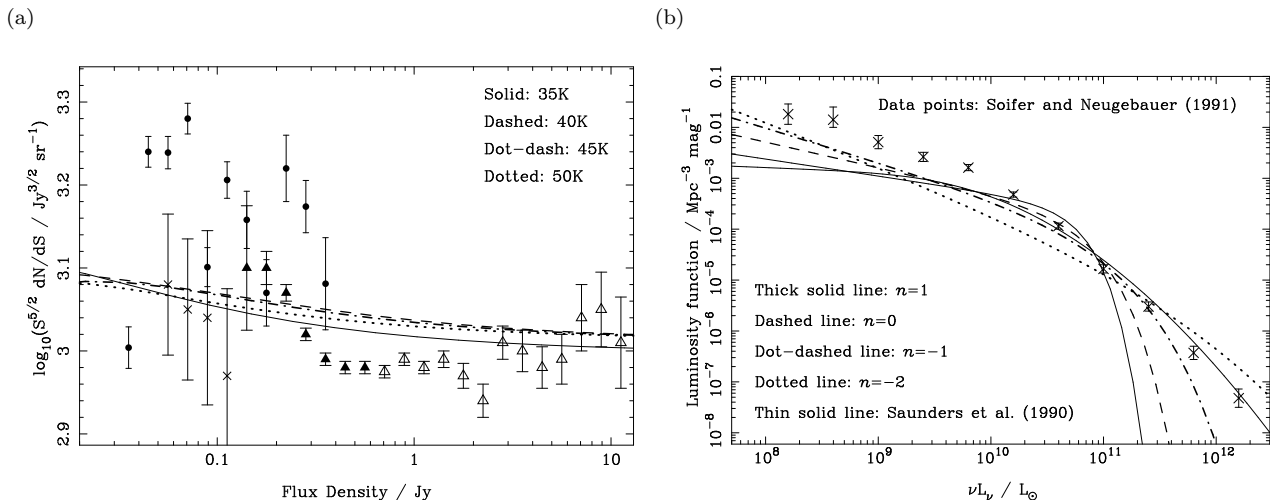


**Figure 4.** (a) Observed 60- $\mu$ m counts of *IRAS* galaxies and the best-fitting models listed in Table 1, plotted in the format used by Oliver, Rowan-Robinson & Saunders (1992). The data are taken from Hacking & Houck (1987; crosses), Rowan-Robinson et al. (1990; empty triangles), Saunders et al. (1990; filled triangles) and Gregorich et al. (1995; circles); see also Bertin, Dennefeld & Moshir (1997). (b) The 60- $\mu$ m luminosity function predicted in the 40-K model, for four different values of the primordial fluctuation index  $n$ . The results are compared with the luminosity function of Saunders et al. (1990) and Soifer & Neugebauer (1991). The luminosity functions derived for the other assumed dust temperatures are very similar.

the self-consistency limits are always satisfied. The details of the calculations can be found in Blain et al. (1999c). It is assumed that all the dust that is generated prior to a particular redshift still existed at that redshift and was available to absorb and reprocess the light from young hot stars and AGN. However, in an hierarchical model, only a small fraction of all the dust generated by any epoch is found in galaxies actively involved in a merger at that epoch; this fraction increases from about 8 to 25 per cent progressively from the 35-K to 50-K model listed in Table 1. Thus, because most of the dust will be found in quiescent objects, the condition in Fig. 5 is less severe than it might be. However, even if only 10 per cent of all dust is involved in a luminous dust enshrouded merger, then the lower limit to the temperature increases only by about 50 per cent, and so this consistency requirement is not difficult to satisfy. The same correction is required if 90 per cent of the energy generated in merging galaxies is attributable to accretion onto AGN, that is, if the AGN fraction  $f_A = 0.9$ . Hence, the models are readily self-consistent if high-redshift Population-III stars exist to generate early metals. More sophisticated models of the coupled evolution of dust, gas and stars have been presented by Pei & Fall (1995), Eales & Edmunds (1996) and Pei et al. (1999).

## 2.6 Metal enrichment and the production of low-mass stars

At the present epoch the density of metals formed by nucleosynthesis in stars  $\Omega_m(0)$  (equation 9) is expected to be about  $10^{-3}$  in the models presented in Table 1. If solar metallicity, about 2.5 per cent by mass (Savage & Sembach 1996), is typical of the Universe as a whole, and the density parameter in baryons  $\Omega_b h^2 = 0.019$  (Burles & Tytler 1998), then  $\Omega_m \simeq 1.9 \times 10^{-3}$  if  $h = 0.5$ . Thus all the models listed in Table 1 are consistent with this limit, even if the AGN fraction

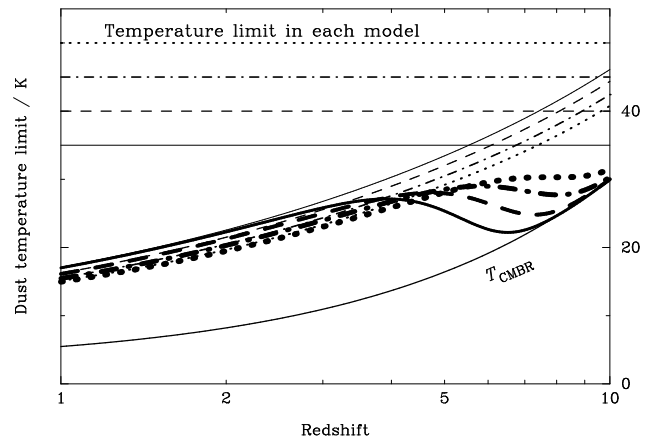


**Figure 5.** The lower limits to the dust temperature as a function of redshift required by the consistency argument discussed in Section 2.5. The dust temperatures in the 35, 40, 45, and 50-K models are shown by the horizontal lines, and the lower limit imposed by the CMBR temperature  $T_{CMBR}$  is shown by the lower solid curve. In a self-consistent model, the lower limit to the temperature must be less than the plotted temperature limits at all epochs. The line styles are the same as those in Figs 3 and 4(a). The four thin lines show the lower limits if no Population III stars are included. The four thick lines show the lower limits if 2 per cent of all star formation activity takes place in a high-redshift Population III.  $z_0 = 20$  in all the models.

$f_A = 0$  and all the luminosity of merging galaxies is due to star formation activity that generates heavy elements.

The density parameter in the form of stars at the present epoch  $\Omega_*(0) = (5.9 \pm 2.3) \times 10^{-3}$  (Gnedin & Ostriker 1992). Observations of Lyman- $\alpha$  absorbers along the line of sight to distant quasars allow the evolution of the mass of neutral gas and the typical metallicity in the Universe to be traced as a function of epoch (Storrie-Lombardi,

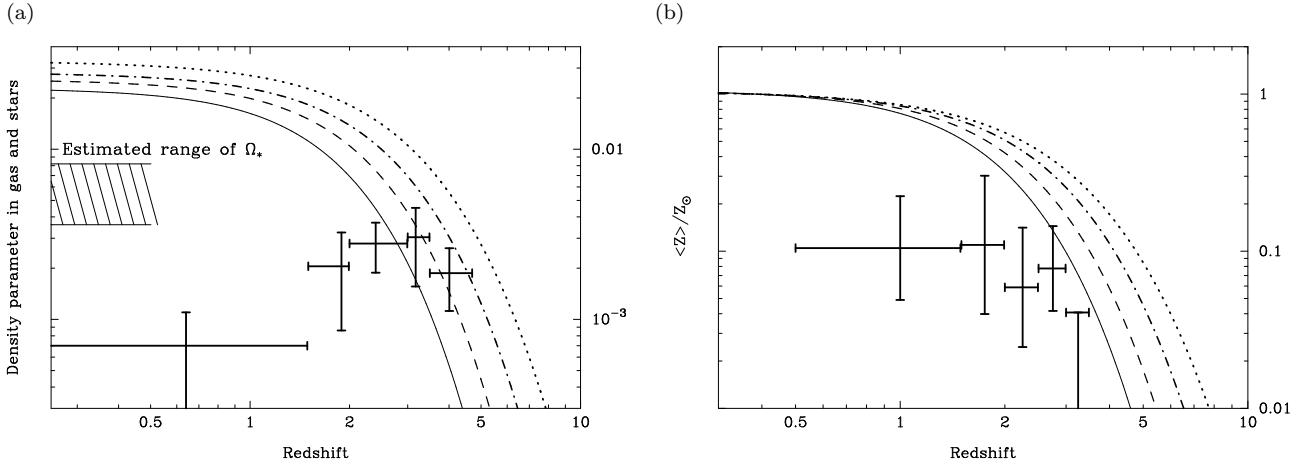


**Figure 6.** (a) The density parameter of gas and stars as a function of redshift. The line styles represent the same models as those in Figs. 3, 4(a) and 5. The curves represent the density parameter of material processed into stars in the models listed in Table 1, assuming a Salpeter IMF with mass limits of  $0.07$  and  $100 M_{\odot}$ . The data for the total density of stars at the present epoch (shaded region) was obtained by Gnedin & Ostriker (1992). The data points represent the density parameter in neutral hydrogen (Storrie-Lombardi et al. 1996). (b) The rate of increase of metallicity expected in the same models, with data from Pettini et al. (1997).

McMahon & Irwin 1996; Pettini et al. 1997). In Fig. 6(a) the mass of material that has been processed into stars is derived as a function of epoch in each of the star-formation histories listed in Table 1, assuming that the AGN fraction  $f_A = 0$  and a Salpeter initial mass function (IMF) with a lower mass limit of  $0.07 M_{\odot}$ . In this case about 65–70 per cent of all stars formed are still burning at the present epoch. The values of  $\Omega_*(0)$  predicted are thus about 3 times larger than the observed value, but are comparable with the values derived in our earlier models (Blain et al. 1999c). In order to account for this difference, either a lower mass limit to the IMF of about  $1 M_{\odot}$  or a value of the AGN fraction  $f_A \simeq 0.75$  is required. This high-mass IMF would be compatible with the inferred lower limit to the IMF of  $3 M_{\odot}$  required by Zepf & Silk (1996) to explain the mass-to-light ratios of elliptical galaxies, and by Rieke et al. (1993) to interpret observations of M82. Stars with masses less than  $3 M_{\odot}$  appear to be less numerous than expected from a Salpeter IMF in recent observations of the low-redshift starburst galaxy R136 (Nota et al. 1998). Goldader et al. (1997) report that the results of near-infrared spectroscopy of nearby *IRAS* galaxies with luminosities between  $10^{11}$  and  $10^{12} L_{\odot}$  support a deficit of stars with masses less than  $1 M_{\odot}$  in these systems. More details about variations in the high-redshift IMF are discussed by Larson (1998).

Metals appear to be overproduced by about a factor of 5 at redshifts of 2 and 3 in the hierarchical models, as shown in Fig. 6(b), but again these results can be reconciled with the observations if a significant fraction of the luminosity of dusty galaxies is being powered by accretion on to AGN. Note, however, that the observations of metallicity could be biased against metal-rich regions of the Universe, either because of their small physical size (Ferguson, Gallagher & Wyse 1998) or because of the complete obscuration of a fraction of background QSOs (Fall & Pei 1993). *ASCA* X-ray observations of significant enrichment in intracluster gas (Mushotzky & Loewenstein 1997; Gibson, Loewenstein &

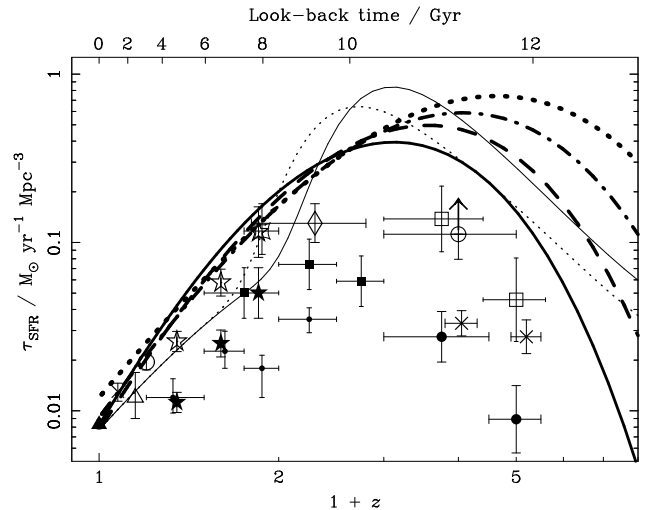


**Figure 7.** The luminosity density predicted by the 35-, 40-, 45- and 50-K models (thick solid, dashed, dot-dashed and dotted lines respectively) listed in Table 1. The values are converted into a star formation rate assuming the same conversion rate as Blain et al. (1999c). References to the points on the plot are listed in the caption of Fig. 1. The thin solid and dotted lines trace the star formation histories derived in Blain et al. (1999c) and Barger et al. (1999b), which were shown in Fig. 1.

Mushotzky 1998), could indicate that this is the case, at least in high-density environments.

The observed turn-over in the neutral gas fraction and the maximum rate of star formation shown in Fig. 6(a) are approximately coincident in redshift, and the rate of enrichment in the hierarchical models is broadly consistent with the slope interpolated between the three highest redshift data points plotted in Fig. 6(b).



## 2.7 The history of star-formation/AGN fuelling

In Fig. 7 the form of evolution of the luminosity density is shown as a function of redshift in the models listed in Table 1. All the models predict curves with a rather similar form at  $z \lesssim 2$ . The transformation between luminosity and star formation rate is the same as that assumed by Blain et al. (1999c): that is, a SFR of  $1 M_{\odot} \text{ yr}^{-1}$  is equivalent to a luminosity of  $2.2 \times 10^9 L_{\odot}$ . At low redshifts the evolution of luminosity density is consistent with optical and near-infrared observations, and with the results presented in our earlier paper.

## 3 SOURCE COUNTS

### 3.1 Fitting the available data

The models presented in Table 1 were constrained using the properties of the counts of the low-redshift 60- $\mu\text{m}$  *IRAS* galaxies. The same formalism can be used to determine the counts of more distant dusty galaxies in the mid-/far-infrared and millimetre/submillimetre wavebands, where a large amount of additional information about the surface density of more distant dusty galaxies is available. There is an upper limit to the surface density of sources at 2.8 mm (Wilner & Wright 1997); counts at 850  $\mu\text{m}$  (Smail et al. 1997; Barger et al. 1998; Holland et al. 1998; Hughes et al. 1998; Barger et al. 1999a; Blain et al. 1999b; Eales et al. 1999); upper limits (Smail et al. 1997; Barger et al. 1998), and a new count (Blain et al. 2000) at 450  $\mu\text{m}$ ; 175- $\mu\text{m}$  *ISO* counts from Kawara et al. (1998) and Puget et al. (1999); 95- $\mu\text{m}$  counts from Kawara et al. (1998); and 7- and 15- $\mu\text{m}$  counts from an extremely deep *ISO* image of Abell 2390 (Altieri et al. 1999), which yields counts that are even deeper than those determined in blank-field surveys by Oliver et al. (1997), Aussel et al. (1999) and Flores et al. (1999).

If the values of the activity parameter at redshift zero,  $(F\sigma)_0^{-1}$ , listed in Table 1 are used to estimate the counts of galaxies at 850 and 175  $\mu\text{m}$ , then the results underpredict the observed counts by a large factor. The form of evolution of the merger efficiency  $x(z)$  is fixed by the observed background radiation intensity, and so, keeping within the framework of our well-constrained models, the value of the activity parameter  $(F\sigma)^{-1}$  at high redshift must be allowed to increase above its value at redshift zero in order to account for the observations. This has the effect of increasing the luminosity of high-redshift mergers, thus increasing the 175- and 850- $\mu\text{m}$  counts. However, the background radiation intensity and the low-redshift 60- $\mu\text{m}$  counts remain unchanged.

The form of evolution of the activity parameter  $(F\sigma)^{-1}$  that is required to explain the data is illustrated in Fig. 8. In Fig. 8(a) the ratio of the model predictions and the observed counts at wavelengths of 175 and 850  $\mu\text{m}$  (Kawara et al. 1998; Blain et al. 1999b respectively) are compared as a function of the activity parameter in the four models listed in Table 1. The same value of the activity parameter cannot account for the observed counts at both wavelengths simultaneously, and the value required to explain the low-redshift 60- $\mu\text{m}$  counts is different from either. The value of the activity parameter required to fit the 60-, 175- and 850- $\mu\text{m}$  counts increases monotonically. Because the median redshift of the

galaxies contributing to the counts at these redshifts is expected to increase monotonically, in Fig. 8(b) we present the ratio of the model predictions and the observed counts as a function of a parameter  $p_{\sigma}$  that describes a simple form of exponential redshift evolution of the activity parameter,

$$(F\sigma)^{-1} = (F\sigma)_0^{-1} \exp p_{\sigma} z. \quad (18)$$

The exponential form provides a reasonable fit to the data, but is only one example of a whole family of potential functions. The important feature is that the function chosen to represent the activity parameter  $(F\sigma)^{-1}$  increases rapidly with increasing redshift.

The zero-redshift value of the activity parameter  $(F\sigma)_0^{-1}$  is fixed by requiring that the low-redshift 60- $\mu\text{m}$  count prediction is in agreement with observations; see Table 1. The values of the evolution parameter  $p_{\sigma}$  that correspond to the most reasonable fit for assumed single dust temperatures of 35, 40, 45 and 50 K are about 1.5, 1.5, 2.0 and 2.3 respectively. If the specific form of the redshift evolution of the activity parameter  $(F\sigma)^{-1}$  shown in equation (18) is assumed, then a dust temperature of 35 or 40 K is most consistent with the data, the same temperature that was required for consistency by both Blain et al. (1999c) and Trentham et al. (1999), and is in agreement with the dust temperatures derived for high-redshift QSOs by Benford et al. (1999).

The increase in the value of the activity parameter  $(F\sigma)^{-1}$  as a function of redshift can be interpreted in terms of two extreme scenarios, or as a combination of both. In the first scenario, the fraction of dark halo mergers that lead to a luminous phase in a dusty galaxy  $F$  is fixed, but that the duration of the luminous phase  $\sigma$  is less at high redshifts. This is plausible, based on the results of simulations of galaxy mergers (e.g. Mihos 1999; Bekki et al. 1999); on average, the typical mass of a merging pair of galaxies is expected to be less at high redshifts in an hierarchical scenario of galaxy evolution, and the gas content of the galaxies is expected to be greater. As a result, the dynamical time of a merger would be expected to decrease with increasing redshift, and the viscosity of the ISM would be expected to increase. Both of these factors might be expected to increase the star formation efficiency of a merger with increasing redshift. In the second scenario, the duration of the luminous phase associated with a merger  $\sigma$  is independent of redshift, but the fraction of mergers that induce such a phase  $F$  is reduced as redshift increases. It is perhaps more plausible that the second of these scenarios could produce the large change in the activity parameter  $(F\sigma)^{-1}$ , by a factor of about 100 from  $z = 0$  to  $z = 3$  that is required to fit the data. This is because the duration of the luminous phase of a merger-induced starburst  $\sigma$  must exceed the lifetime of a reasonably massive star, i.e.  $\sigma \gtrsim 10^7$  yr. If star formation activity powers a significant fraction of the SCUBA galaxies, as seems reasonable, then this limit to the value of the merger duration  $\sigma$  is constrained to be greater than about  $10^7$  yr, only a few times less than the values of  $\sigma$  at  $z = 0$  listed in Table 1. Thus it seems likely that a large fraction of the increase in the value of the activity parameter  $(F\sigma)^{-1}$ , which is required at high redshifts to account for the observed counts, should be attributed to a reduction in the fraction  $F$  of dark halo mergers that generate a luminous galaxy. We speculate that this may be connected with the lower typical metallicity ex-

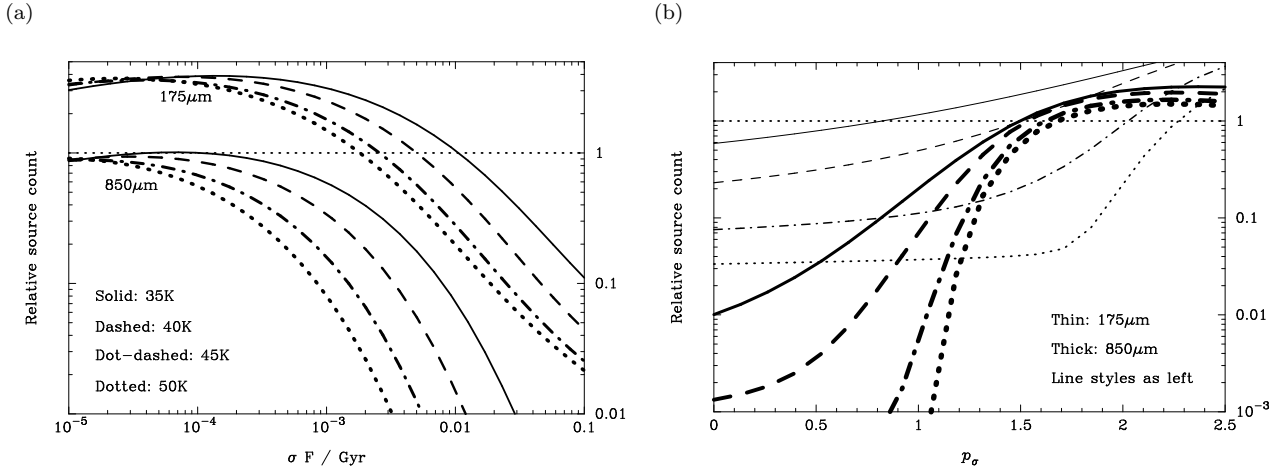


**Figure 8.** The ratio of the counts predicted by the four models listed in Table 1, and the observed counts, at 175 and 850  $\mu\text{m}$  (Kawara et al. 1998; Blain et al. 1999b respectively). The upper limits to the counts at 450  $\mu\text{m}$  and 2.8 mm are never violated. In (a) the ratio is shown as a function of the reciprocal of the activity parameter  $F\sigma$ , which is fixed as a function of redshift; in (b) the ratio is shown as a function of  $p_\sigma$ , the exponent in equation (18), which describes the exponential evolution of the activity parameter  $(F\sigma)^{-1} \propto (F\sigma)_0^{-1} \exp p_\sigma z$ . Clearly, strong redshift evolution of the activity parameter in merging galaxies is required in order to fit the counts at long wavelengths.

pected at higher redshifts. In a lower metallicity system the cooling of dense gas would be expected to be less efficient, and so a large amount of high-mass star formation may be unable to take place during the short merger process.

### 3.2 Predicted counts of dusty galaxies

Counts predicted by the four models listed in Table 1, employing the values of  $p_\sigma$  listed above, are compared with observations at wavelengths of 15, 60, 175, 450, 850, 1300 and 2800  $\mu\text{m}$  in Fig. 9. While these models do not present unique solutions, fewer parameters are involved in the model than the number of separate pieces of constraining data. In future, by comparing the predictions of the models with observations, especially with the redshift distributions of the SCUBA galaxies (Barger et al. 1999b; Lilly et al. 1999; Smail et al. 1999, in preparation), the models can be developed to account more accurately for the increasing amount of available data.

### 3.3 The corresponding radio counts

There is a tight correlation between the flux densities of low-redshift galaxies in the radio and far-infrared wavebands (see the review by Condon 1992). Thus the counts of faint galaxies observed in the radio waveband should not be overproduced when the SEDs of the galaxies in the 35-, 40-, 45- and 50-K models presented here are extended into the radio waveband using this correlation. It is permissible to underpredict the counts, as there will be a contribution from AGN to the faint counts, which need not be associated with powerful restframe far-infrared emission from dust. Partridge et al. (1997) report a 8.4-GHz galaxy count of  $1.0 \pm 0.1 \text{ arcmin}^{-2}$  brighter than a flux density of  $10 \mu\text{Jy}$ . The correspondings count predicted by the 35-, 40-, 45- and 50-K models are 0.6, 0.7, 1.0 and 0.6  $\text{arcmin}^{-2}$  respectively. Thus all the models discussed here are consistent with the deep radio observations. For comparison, a count of 0.8  $\text{arcmin}^{-2}$  is predicted

by the modified Gaussian model discussed in Barger et al. (1999b), which is modified from the results of the simple luminosity evolution models presented by Blain et al. (1999c).

### 3.4 Redshift distributions

The redshift distributions of submillimetre-selected sources at, or just below, the flux density limits of current surveys have been discussed by Blain et al. (1999c) in the context of models of a strongly evolving population of distant dusty galaxies, based on the low-redshift *IRAS* galaxy luminosity function. The first spectroscopic observations of a large fraction of the potential optical counterparts to SCUBA galaxies identified in deep multicolour optical images (Smail et al. 1998) have been made by Barger et al. (1999b) (see Fig. 10). This redshift distribution is consistent with the optical identifications made by Lilly et al. (1999) in a SCUBA survey of Canada–France Redshift Survey (CFRS) fields. The distribution shown in Fig. 10 is, however, subject to potential misidentifications of SCUBA galaxies. For example, recent deep near-infrared images show that two of the Smail et al. (1998) SCUBA galaxies, which were originally identified with low-redshift spiral galaxies, can more plausibly be associated with extremely red objects (EROs) that were unidentified in optical images (Smail et al. 1999). In two other cases, at  $z = 2.55$  (Ivison et al. 1999) and  $z = 2.81$  (Ivison et al. 1998), the identifications have been confirmed by detections of redshifted CO emission (Frayser et al. 1998; 1999), and in another case spectroscopy and *ISO* observations (Soucail et al. 1999) strongly support the identification of a ring galaxy at  $z = 1.06$ .

The preliminary redshift distribution of SCUBA galaxies, shown in Fig. 10, is broadly consistent with the predictions of the Gaussian model of Blain et al. (1999c). A modified Gaussian model, as shown in Fig. 1, was described by Barger et al. (1999b); the values of the evolution parameters in the modified Gaussian model were explicitly fitted both to the background radiation intensity and count data

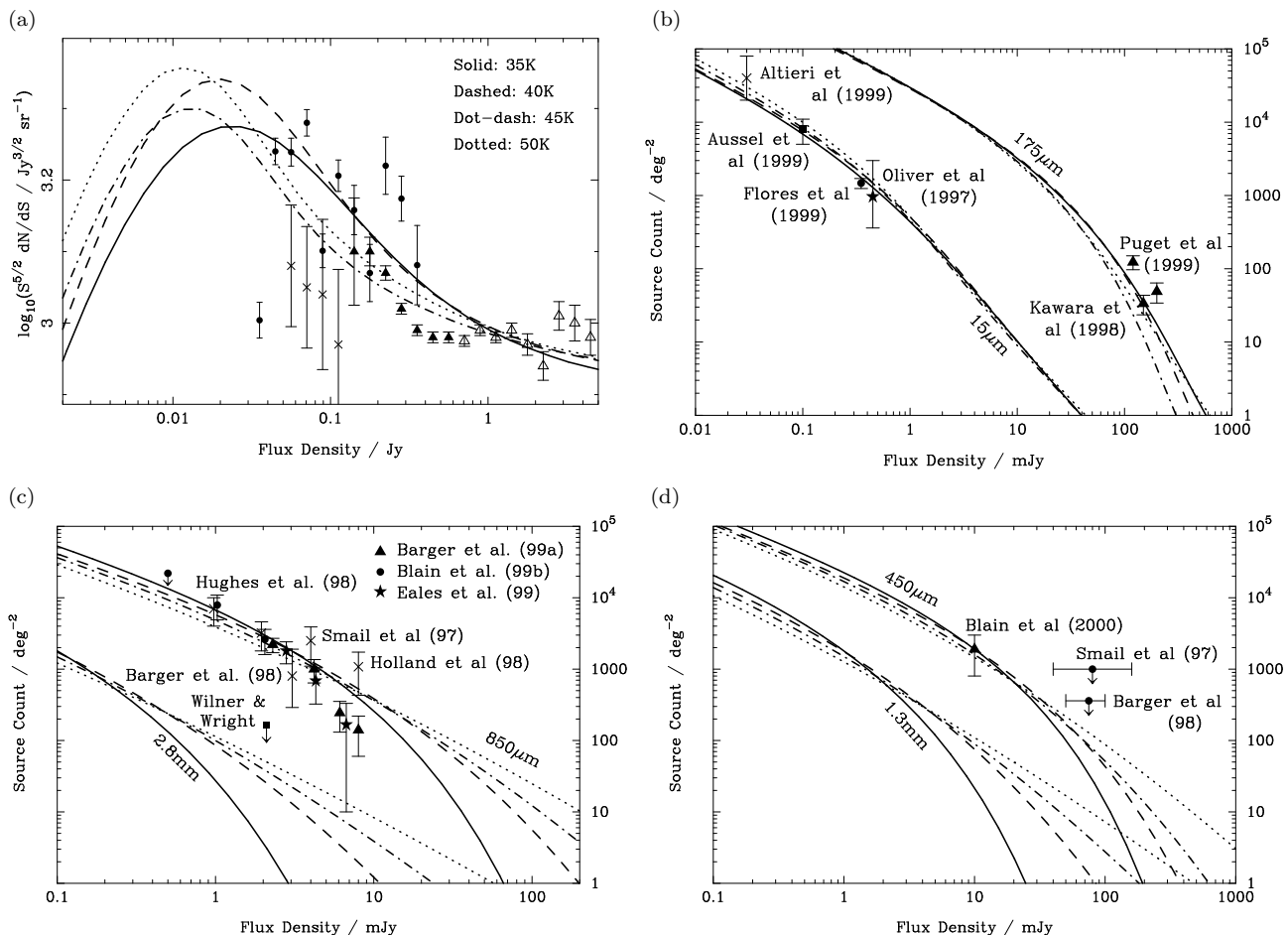


**Figure 9.** Counts predicted by the models listed in Table 1, compared with available data. The 60- $\mu$ m counts are shown in (a), those at 15 and 175  $\mu$ m are shown in (b), those at 850  $\mu$ m and 2.8 mm are shown in (c), and those at 450  $\mu$ m and 1.3 mm are shown in (d). The references to the data in (a) are given in the caption of Fig. 4(a); in (b), (c) and (d) they are written adjacent to the data points.

and to the observed median redshift. In Fig. 10 the observed redshift distribution is compared with the redshift distributions predicted in the Gaussian and modified Gaussian models, and with the predictions of the hierarchical models developed here (see Table 1). Median redshifts of about 2.2, 2.7, 3.2 and 3.5 are expected in the 35-, 40-, 45- and 50-K hierarchical models respectively.

The redshift distributions predicted by the hierarchical models have median redshifts greater than that in the modified Gaussian model, but less than those in either the other models presented by Blain et al. (1999c) or the hierarchical model E from Guiderdoni et al. (1998), all of which provide a reasonable fit to both the background radiation intensity and source counts in the far-infrared/submillimetre waveband. Based on these results, the coolest 35-K model seems to be in best agreement with the available data. A model in which the single-temperature dust clouds discussed here are replaced by a temperature distribution will probably be required to account for the redshift distribution of the SCUBA galaxies. When the two spiral galaxies at  $z < 0.5$  are replaced by EROs at  $z > 1$  (Smail et al. 1999), the agreement between the 35-K hierarchical prediction and the observed redshift distribution is rather satisfactory.

In all the hierarchical models, despite strong negative

evolution of the mass-to-light ratio of mergers with increasing redshift, most of the detected galaxies are expected to lie at redshifts less than 5, and so will be accessible to multi-wavelength study using 8-m class telescopes. When final reliable identifications and redshifts for submillimetre-selected galaxies are available, this information will be crucial for refining the hierarchical model.

#### 4 OPTICAL BACKGROUNDS AND COUNTERPARTS

The discussion has so far centred on the properties of merging galaxies as observed through their dust emission in the mid-infrared, far-infrared and millimetre/submillimetre wavebands. Here we assume the same forms of evolution of both the merger efficiency parameter  $x$  and the activity parameter  $(F\sigma)^{-1}$  that were required to account for the data in the far-infrared and submillimetre wavebands in the previous section, but make predictions in the near-infrared, optical and ultraviolet wavebands. In particular, we investigate the 35-K model, in which the redshift distribution of SCUBA galaxies is in best agreement with observations.

Subject to the uncertain fraction of the luminosity of

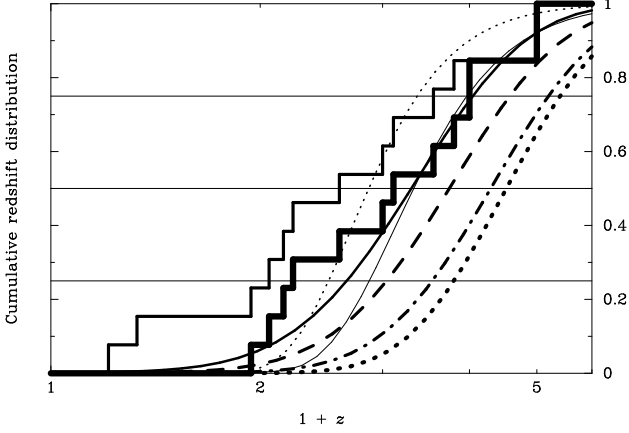


**Figure 10.** The redshift distributions of 850- $\mu\text{m}$  galaxies in the Smail et al. (1998) sample predicted in the 35-, 40-, 45- and 50-K hierarchical models listed in Table 1 (thick smooth lines; solid, dashed, dot-dashed and dotted respectively), the Gaussian model (thin smooth solid line; Blain et al. 1999c) and the modified Gaussian model (thin dotted line; Barger et al. 1999). The modified Gaussian model is fitted to the median redshift of the preliminary redshift distribution determined by Barger et al. (1999b) for the optical counterparts to submillimetre-selected galaxies (Smail et al. 1998), which is shown by the thinner jagged solid line. Sources with no optical counterparts are assumed to be at  $z = 4$ . Using subsequent  $K$ -band observations, Smail et al. (1999) have modified the identifications of the counterparts of the two galaxies at  $z < 1$  in the sample, from low-redshift spirals to high-redshift EROs. After this modification, the revised redshift distribution is shown by the thicker jagged solid line, if the EROs are both assumed to lie at  $z = 3$ .

these galaxies that is assumed to be powered by star formation activity, we predict the integrated background radiation intensity from the near-infrared to ionizing ultraviolet wavebands, and the counts of galaxies with SEDs that are dominated by evolved stars in the near-infrared  $K$ -band, and by young stars in the optical  $B$ -band. By requiring that the  $K$ - and  $B$ -band counts are reproduced accurately, we estimate both the fraction of all energy released in mergers that is reprocessed by dust  $A$  and the normalization of the activity parameter at  $z = 0$ ,  $(F\sigma)_0^{-1}$  in the optical waveband. For a discussion of the evolution of faint galaxies and their stellar populations see Ellis (1997).

#### 4.1 $K$ -band counts

The counts of galaxies in the  $K$ -band at a flux density  $S_K$  can be predicted by assuming the forms of the merger efficiency  $x(z)$ , as listed in Table 1, an SED typical of evolved stars  $f_\nu^K$  (Charlot, Worthey & Bressan 1996), the Press–Schechter mass function (equation 1) and the mass-to-light ratio of evolved stellar populations  $R_{\text{ML}}$ . The SED was calculated using a 9.25-Gyr old Bruzual–Charlot instantaneous burst model with a Salpeter IMF. Upper and lower mass limits of 0.1 and 125  $M_\odot$  were assumed for the IMF. Note that the form of the evolved stellar spectrum derived is almost independent of the exact values of the upper and lower mass limits assumed. The  $K$ -band count

$$N_K(S_K) = \int_0^{z_0} \int_{M_K(z)}^\infty N_{\text{PS}}(M) dM D(z)^2 \frac{dr}{dz} dz, \quad (19)$$

with

$$M_K(z) = 4\pi D^2(1+z) S_K R_{\text{ML}}(z) \frac{\int f_{\nu'}^K d\nu'}{f_{\nu_K}^K(1+z)}. \quad (20)$$

By ensuring that the predicted counts match the observed  $K$ -band counts, a suitable form of the mass-to-light ratio  $R_{\text{ML}}$  is determined as a function of redshift. The mass in this ratio is defined as the mass of the dark matter haloes of galaxies, taken from the Press–Schechter function (equation 1), and the luminosity is the bolometric luminosity of the evolved stellar population in the galaxies.

In order to reproduce the observed  $B$ -band counts, the counts derived for the evolved and merging components are added together, as shown in Fig. 11(b). The redshift dependence of the mass-to-light ratio is the same as that of the luminosity density of evolved stars,

$$\epsilon_L(z) \propto \frac{1}{1+z} \frac{\int_0^{z_0} \frac{x(z') dz'}{1+z'}}{\int_z^{z_0} \frac{x(z') dz'}{1+z'}}, \quad (21)$$

which depends on the SFR at all earlier epochs. A factor of  $1+z$  is included in the denominator to mimic the effects of passive stellar evolution (Longair 1998). At  $z = 0$  a form of the mass-to-light ratio,

$$\frac{R_{\text{ML}}}{M_\odot L_\odot^{-1}} = \begin{cases} 80, & \text{if } L_{10} \geq 2; \\ 117 L_{10}^{-0.55}, & \text{otherwise,} \end{cases} \quad (22)$$

where  $L_{10} = L/10^{10} L_\odot$ , is required to match the observed  $K$ -band counts (Fig. 11a) and the faint-end slope of the observed  $K$ -band luminosity function (Gardner et al. 1996; Szokoly et al. 1998).

The well fitting  $K$ -band count that is derived from the model with this form of the mass-to-light ratio  $R_{\text{ML}}$  is shown, along with the observational data, in Fig. 11(a).

#### 4.2 $B$ -band counts

Both passive evolved galaxies and luminous merging galaxies make a contribution to the  $B$ -band counts. The evolved contribution is predicted by evaluating the function that produces the  $K$ -band count at the frequency of the  $B$ -band. The extrapolation is made using the model SED described above. An additional population of merging galaxies is also included. Their counts are determined using equation (13) directly, with a value of

$$M_{\text{min}} = \frac{1}{1-A} \frac{4\pi D^2(1+z) S_B}{0.007c^2} \frac{F\sigma}{x(z)} (1-f_A) \frac{\int f_{\nu'}^B d\nu'}{f_{\nu_B}^B(1+z)}. \quad (23)$$

$A$  is the fraction of the total energy released in a merger that is reprocessed into the far-infrared waveband, and  $f_\nu^B$  is the SED of a flat star-forming young stellar spectrum at frequencies less than the Lyman limit frequency  $\nu_{\text{Ly}} = 3.3 \times 10^{15}$  Hz.  $f_\nu^B \propto \nu^0$  if  $\nu \leq \nu_{\text{Ly}}$  and zero otherwise. The blue power-law SED expected from an AGN will be described reasonably well by this SED at  $\nu < \nu_{\text{Ly}}$ .

The faint counts at  $B > 21$ , which are dominated by merging galaxies, can be reproduced in the model only if the dust absorption fraction  $A \simeq 0.8$  and the zero-redshift

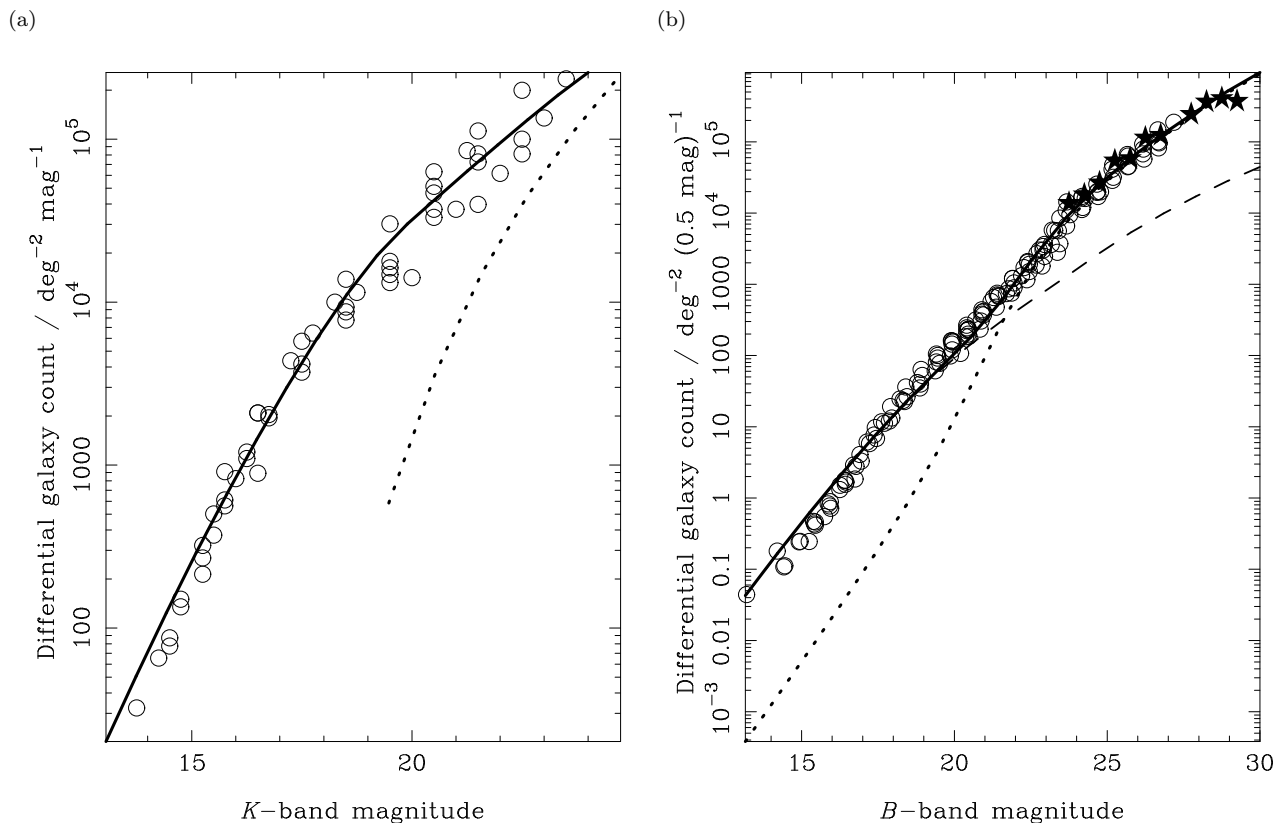


**Figure 11.** (a) Near-infrared  $K$ -band and (b) optical  $B$ -band counts predicted in the 35-K hierarchical model (Table 1). The  $K$ -band counts are produced almost entirely by quiescent non-merging galaxies (solid line). If the flat spectra of the merging galaxies are extrapolated into the  $K$  band, as shown by the dotted line, then the counts would be expected to increase by about 10 per cent at  $K = 20.5$  and by 30 per cent at  $K = 23$ . In the  $B$ -band, the total counts (solid line) are dominated at the bright end by the small hot stellar component of the quiescent galaxies (dashed line), and at the faint end by the young stellar populations of flat-spectrum merger induced starbursts/AGN (dotted line). Data points obtained using ground-based telescopes are shown by open circles; data points from the *Hubble Space Telescope* are shown by filled stars. The data are taken from the compilation of Metcalfe et al. (1996).

activity parameter  $(F\sigma)_0^{-1} = 2.5 \text{ Gyr}^{-1}$ . The activity parameter incorporated in the model evolves with redshift as shown in equation (18), with the value of  $p_\sigma = 1.5$  that is appropriate in the 35-K model. Note that this value of the activity parameter is less than that required to account for the observed submillimetre-wave counts, and that the ratio of energy emitted in the restframe ultraviolet and far-infrared wavebands is 1:4. This ratio is equivalent to 1.75 magnitudes of extinction when integrated over the optical and ultraviolet wavebands.

The redshift distribution of faint galaxies at  $z \gtrsim 1$  derived in the hierarchical model is in good agreement with that observed for galaxies with  $B < 24$  (Cowie, Hu & Songaila 1995); these details are discussed more extensively elsewhere (Jameson et al. 1999, in preparation). Note that the dependence of the submillimetre and faint  $B$ -band counts on the merging efficiency parameter  $x(z)$  and the AGN fraction  $f_\Lambda$  is identical, and so the value of the AGN fraction does not affect the resulting counts.

The most numerous population of faint high-redshift optically selected galaxies known are the Lyman-break galaxies (Steidel et al. 1996a, 1999) at  $2.5 \geq z \geq 4.5$ , which have apparent SFRs of a few  $10 M_\odot \text{ yr}^{-1}$ . The surface density of detected Lyman-break galaxies is about an order of magnitude greater than that of submillimetre-selected

galaxies, while their SFRs are typically about an order of magnitude less.

The violence of a typical merger-induced starburst/AGN, and thus its detectability, is determined by the product of the merging efficiency and activity parameters,  $x(F\sigma)^{-1}$ , in the hierarchical model. The value of this composite parameter that is required to fit the observed submillimetre-wave counts is about 40 times greater than that required to fit the faint  $B$ -band counts. The value of the activity parameter  $(F\sigma)^{-1}$  that is required to fit the submillimetre-wave counts is a factor of about 10 times greater than that required to fit the  $B$ -band counts. These differences are thus comparable with the observed ratios of the surface densities and luminosities of typical galaxies in the submillimetre-selected and Lyman-break samples.

Based on these differences, we suggest a scenario in which the optically selected Lyman-break galaxies and the submillimetre-selected SCUBA galaxies are drawn from the same underlying population of luminous galaxy merger events, but are distinguished by being observed during two distinct phases of the merger process. We associate one phase, which is very luminous, short-lived and heavily dust enshrouded, with the SCUBA galaxies, and the other, which is less luminous and relatively lightly obscured, with the Lyman-break galaxies. During the first phase, which is about

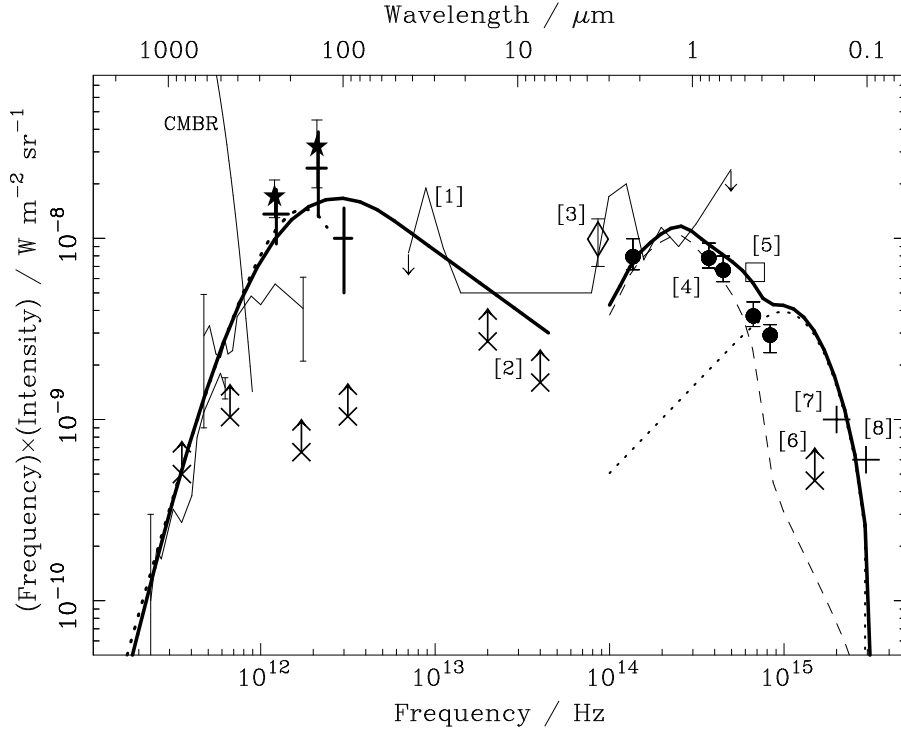


**Figure 12.** The background radiation intensity in the hierarchical models from the millimetre to the ultraviolet waveband. The thick solid line shows the total background radiation intensity predicted in the 35-K model (Table 1). In the near-infrared/optical/ultraviolet waveband the separate contributions to the background intensity from the old stellar population (dashed line) and the young stellar population/AGN (dotted line) are also shown. At long wavelengths the data points are identical to those plotted in Fig. 3. Other measurements are numbered: 1. Stanev & Franceschini (1998); 2. Altieri et al. (1999); 3. Dwek & Arendt (1998); 4. Pozzetti et al. (1998); 5. Toller, Tanabe & Weinberg (1987); 6. Armand, Milliard & Deharveng (1994); 7. Lampton, Bowyer & Deharveng (1990); and 8. Murthy et al. (1999); see also Bernstein, Freedman & Madore (1999), who determine a greater absolute background radiation intensity in the optical waveband.

40 times more luminous, but only about a tenth of the duration as compared with the second, most of the activity in the merger will be almost completely obscured from view in the optical waveband, but extremely bright in the submillimetre waveband. This phase is consistent with the extremely compact nuclear starburst/AGN activity observed by Downes & Solomon (1998) on sub-kpc scales in nearby ultraluminous *IRAS* galaxies. During the second phase, less intense star formation activity would probably be distributed throughout the ISM of both merging galaxies. A short lived ultraluminous phase and a longer-lived less intense burst of star formation activity during a merger are consistent with the results of hydrodynamic models of galaxy mergers by Mihos & Hernquist (1996) and Bekki et al. (1999).

However, while plausible, this scenario is not necessarily correct. The faint counts in the submillimetre and optical waveband could simply be drawn from two distinct populations. The questions of whether and how ultraluminous dust-enshrouded mergers are connected with the Lyman-break galaxies can only be answered by making multiwaveband observations of large samples of submillimetre-selected galaxies in order to observe a time sequence of merging galaxies and to investigate the merger process in detail. Observations of the Lyman-break population in the submillimetre waveband (Chapman et al. 1999) will also help to address these questions.

### 4.3 Integrated background light

The global luminosity density predicted by the hierarchical models is based on the evolution of the merging efficiency parameter  $x(z)$ . By making minor modifications to the formalism presented in Section 2.3, the models listed in Table 1 can be used to predict the background radiation intensity.

The near-infrared/optical/ultraviolet background radiation intensity produced by merging galaxies can be calculated as shown in equation (11), if the fraction of energy generated by a merger that is absorbed by dust  $A$  is included. Thus

$$I_{\nu}^{\text{opt}} \propto (1-A) \frac{\phi}{\gamma\sqrt{\alpha}} \int_0^{z_0} \frac{x(z)}{1-f_A} \frac{\dot{\delta}(z)}{\delta(z)} \frac{f_{\nu(1+z)}^B}{\int f_{\nu'}^B d\nu'} \frac{dr}{dz} \frac{dz}{1+z}. \quad (24)$$

The background radiation intensity due to the evolved stellar population is not given directly by the expression for the far-infrared background in equation (11). In that case the volume emissivity is given by equations (21) and (22). By integrating this emissivity of evolved objects over redshift, assuming the SED  $f_{\nu}^K$  introduced above, the background radiation intensity produced by evolved non-merging galaxies can be calculated. When it is added to the background radiation spectrum produced in merging galaxies, a complete prediction of the background intensity between the near-infrared and near-ultraviolet wavebands is obtained.

The background radiation intensity predicted using the 35-K model, which can explain the  $K$ - and  $B$ -band galaxy

counts, is shown across the millimetre to the ultraviolet wavebands in Fig. 12. The background intensity is in agreement with almost all the observed limits and detections. The only spectral region in which the background radiation intensity is still not very well defined is between about 3 and  $7\ \mu\text{m}$ . At these wavelengths, the dominant source of background radiation switches from dust emission to starlight. There is almost certainly an additional, and perhaps dominant, contribution to the background radiation intensity in the mid-infrared waveband from very hot dust grains in the central regions of AGN, which are not modelled here. The model curves shown Fig. 12 are not extrapolated into this region from the well-determined populations of galaxies at  $60\text{-}\mu\text{m}$  and in the  $K$  band.

## 5 OVERVIEW OF MODEL PARAMETERS

We have introduced a series of parameters and functions to account for different observations section by section through the paper. Excluding the world model parameters  $H_0$ ,  $\Omega_0$  and  $\Omega_\Lambda$ , five parameters are required to define the merger rate of dark matter haloes. Five further independent parameters [ $x_0$ ,  $p$ ,  $z_{\text{max}}$ ,  $(F\sigma)_0^{-1}$  and  $p_\sigma$ ] and a SED for dusty galaxies, are required to fit the counts at wavelengths of 15, 60, 175, 450 and  $850\ \mu\text{m}$  and the submillimetre-wave/far-infrared background radiation spectrum. The most important element of the models are the two functions that describe the merger efficiency parameter  $x(z)$  and the activity parameter  $(F\sigma)^{-1}$ . We present appropriate forms for these functions in equations (16) and (18) respectively, but stress that these forms are not unique. As more data becomes available, other functional forms or free-form fitting functions may be more appropriate. By modifying the activity parameter  $(F\sigma)_0^{-1}$ , introducing the total fraction of luminosity absorbed by dust  $A$ , and including a template SED for star-forming galaxies in the rest frame ultraviolet waveband, the  $B$ -band counts can also be reproduced. In Table 2 we summarize these parameters and the most important pieces of data used to constrain them. The values of the parameters required to fit the data in the 35-K model are also listed.

## 6 CONCLUSIONS

(i) We have presented a simple model of hierarchical galaxy formation which incorporates the effects of obscuration by dust, in which the galaxies that are detected in submillimetre-wave surveys are observed during a merger-induced episode of star formation or AGN fuelling. The aim of this model is to elucidate the most important physical processes that could be at work in luminous dusty galaxies, rather than to provide a detailed quantitative description.

(ii) The model is constrained primarily by the intensity of background radiation in the far-infrared/submillimetre waveband. From these data alone, the luminosity density from high-redshift galaxies is inferred to exceed that deduced from observations in the rest frame ultraviolet and optical wavebands by up to an order of magnitude. The source counts and background radiation intensity in the submillimetre, far-, mid- and near-infrared, and optical wavebands

are reproduced adequately in the model without introducing a large number of parameters.

(iii) The counts of galaxies detected in the far-infrared/submillimetre and optical wavebands, and the associated background radiation intensities in these wavebands are consistent if about 4 times more energy is emitted by galaxies after being reprocessed into the far-infrared waveband by interstellar dust as is radiated directly in the optical/ultraviolet waveband.

(iv) In order to account for the observed abundance of distant galaxies detected at 175 and  $850\ \mu\text{m}$  using *ISO* and SCUBA, the mass-to-light ratio of a typical galaxy merger must decrease with redshift, by a factor of about 10 and 200 at  $z = 1$  and 3 respectively. Thus high-redshift mergers must be typically more violent as compared with their low-redshift counterparts. We suggest two possible physical explanations. First, that gas is converted into stars/feeds an AGN uniformly more efficiently and rapidly in all merging galaxies as redshift increases, perhaps due to a lower bulge-to-disk ratio, which makes disk instabilities grow more quickly (Mihos & Hernquist 1996). Secondly, that a decreasing fraction of dark matter halo mergers are associated with an efficient mode of star formation/AGN fuelling as redshift increases.

(v) In the context of galaxy formation within merging dark matter haloes, we have described how the physical processes that convert merging mass into visible radiation must evolve with redshift in order to account for the data in the far-infrared and submillimetre wavebands. This has previously been discussed by Guiderdoni et al. (1998), in the conventional context of semi-analytic models, where gas is assumed to cool into dark matter haloes and form stars on galactic scales. In order to account for the observations, an additional population of ultraluminous galaxies was incorporated arbitrarily into their models. We have improved our previous models (Blain et al. 1999c) significantly, by including some astrophysics and not simply invoking an empirical form of the evolution of a low-redshift luminosity function to fit the data. By assuming only a single population of luminous merging galaxies we are able to account for all the data in the far-infrared and submillimetre wavebands. Clear forms of evolution of both the efficiency with which luminosity is generated by a galaxy merger as a function of redshift, and of a function that connects the duration of the luminous phase and the fraction of dark matter halo mergers that generate a luminous event are required to reproduce the results of observations. The way in which gas is processed in the sub-kpc core regions of galaxy mergers to reproduce the necessary high efficiency and short time-scale of luminous events must be investigated in future work.

(vi) We find that the observed counts of both submillimetre-selected galaxies and Lyman-break galaxies can be accounted for in terms of merger events in an hierarchical model of galaxy formation, which include identical forms of evolution with redshift, but with different absolute normalisations. We find that 80 per cent of the total amount of energy generated in merger-induced starbursts/AGN is liberated in the far-infrared waveband. It is plausible that the submillimetre-selected galaxies and the Lyman-break galaxies are associated with temporally distinct phases of a common population of merging dark matter haloes. A scenario in which a short-lived, highly obscured

**Table 2.** A summary of the parameters and functions that have been introduced in this paper, generally listed in order of their first appearance. The values of these parameters in the best-fitting 35-K model, which reproduces the current redshift distribution of submillimetre-selected galaxies adequately, are also listed. An Einstein-de Sitter world model with  $h = 0.5$  is assumed throughout.

Name	Symbol	Value in the 35-K model	Constrained by
Smoothed density	$\bar{\rho}$	N/A	Assumed equivalent to $\Omega_0 = 1$
Fluctuation index	$n$	$n \simeq -1$	60- $\mu\text{m}$ luminosity function
	$\gamma = 1 + (n/3)$		
Fluctuation mass ( $z = 0$ )	$M^*$	$3.6 \times 10^{12} M_\odot$	Tully-Fisher relation
Merger rate constants	$\phi, \alpha$	1.7, 1.4	Self-similar merging process
Far-infrared SED	$f_\nu$	N/A	4 temperatures assumed
Fraction of luminous mergers powered by AGN	$f_A$	$f_A = 0$ (generally assumed)	see Section 2.3
Timescale of mergers	$\sigma$	N/A	see activity parameter
Fraction of mergers that yield luminous events	$F$	N/A	see activity parameter
Merger star-formation efficiency	$x(z)$ (equation 16)	$x_0 \simeq 10^{-4}(\gamma^2 F \sigma)^{1/3}(1 - f_A) \text{Gyr}^{-1/3}$ $p = 4.4$ $z_{\text{max}} = 0.44$	Bright 60- $\mu\text{m}$ counts Far-infrared background Far-infrared background
Activity parameter (submillimetre/far-infrared)	$(F\sigma)^{-1}(z)$ (equation 18)	$(F\sigma)_0^{-1} = 18.8 \text{Gyr}^{-1}$ $p_\sigma \simeq 1.5$	Bright 60- $\mu\text{m}$ counts 175- and 850- $\mu\text{m}$ counts
Activity parameter ( $B$ -band)		$(F\sigma)_0^{-1} = 2.5 \text{Gyr}^{-1}$ $p_\sigma \simeq 1.5$	Faint $B$ -band counts From submillimetre results
Fraction of energy that is reprocessed by dust	$A$	0.8	Faint $B$ -band counts
$B$ - and $K$ -band SEDs	$f_\nu^B, f_\nu^K$	N/A	Spectral synthesis models
Mass-to-light ratio of evolved galaxies	$R_{\text{ML}}$	See equation (22)	$K$ -band counts

far-infrared starburst/AGN phase dominates the integrated luminosity of the merger and is surrounded in time by a less luminous, more lightly obscured phase that lasts about 10 times longer is consistent with the data. In this scenario, the merger would be classified as a SCUBA galaxy if it was observed during the short-lived phase, and as a Lyman-break galaxy during the long-lived phase.

(vii) The results presented here provide excellent opportunities for further study. Two key scientific questions remain unanswered. First, what are the physical processes that are responsible for the evolution of both the star-formation/AGN-fuelling efficiency and the activity parameter in galaxy mergers as a function of redshift? Secondly, what is the relationship between samples of faint galaxies selected in the optical waveband and submillimetre-selected galaxies? Larger samples of submillimetre-selected galaxies and more comprehensive multiwaveband follow-up observations will allow these questions to be answered.

## ACKNOWLEDGEMENTS

We thank Nigel Metcalfe for providing a comprehensive list of optical count data, and Chris Mihos, Priya Natarajan, Kate Quirk, Chuck Steidel and Neil Trentham for providing useful comments on the manuscript. Thanks are also due to an anonymous referee for helpful suggestions and prompt reading of the manuscript. AWB, AJ and RJI acknowledge PPARC, IS thanks the Royal Society, and JPK thanks the CNRS for support. In addition, AWB thanks MENRT for

support while in Toulouse, and the Caltech AY visitors program for support while this work was completed.

## REFERENCES

- Almaini O., Lawrence A., Boyle B. J., 1999, MNRAS, 305, L59  
 Altieri B. et al., 1999, A&A, 343, L65  
 Armand C., Milliard B., Deharveng J. M., 1994, A&A, 284, 12  
 Aussel H., Cesarsky C. J., Elbaz D., Starck J.-L., 1999, A&A, 342, 313  
 Barger A. J., Cowie L. L., Sanders D. B., Fulton E., Taniguchi Y., Sato Y., Kawara K., Okuda H., 1998, Nat, 394, 248  
 Barger A. J., Cowie L. L., Sanders D. B., 1999a, ApJ, 518, L5  
 Barger A. J., Cowie L. L., Smail I., Ivison R. J., Blain A. W., Kneib J.-P., 1999b, AJ, 117, 2656  
 Baugh C. M., Cole S. M., Frenk C. S., Lacey C. G., 1998, ApJ, 498, 504  
 Bekki K., Shioya Y., Tanaka I., 1999, ApJ, 520, L99  
 Benford D. J., Cox P., Omont A., Phillips T. G., 1999, ApJ, 518, L65  
 Bernstein R., Freedman W., Madore B., 1999, ApJ, submitted  
 Bertin E., Dennefeld M., Moshir M., 1997, A&A, 323, 685  
 Blain A. W., Longair M. S., 1993a, MNRAS, 264, 509  
 Blain A. W., Longair M. S., 1993b, MNRAS, 265, L21  
 Blain A. W., Longair M. S., 1996, MNRAS, 279, 847  
 Blain A. W., Möller O., Maller A. H., 1999a, MNRAS, 302, 423  
 Blain A. W., Kneib J.-P., Ivison R. J., Smail I., 1999b, ApJ, 512, L87  
 Blain A. W., Smail I., Ivison R. J., Kneib J.-P., 1999c, MNRAS, 302, 632  
 Blain A. W., Ivison R. J., Kneib J.-P., Smail I., 2000, in Bunker



- A., van Breughel W. eds, The Hy-Redshift Universe, Astron. Soc. Pac., San Francisco, in press (astro-ph/9908024)
- Brainerd T. G., Villumsen J. V., 1992, *ApJ*, 394, 409
- Burles S., Tytler D., 1998, *ApJ*, 499, 699
- Chapman S. C. et al., 1999, *MNRAS*, submitted
- Charlot S., Worthey G., Bressan A., 1996, *ApJ*, 457, 625
- Cole S. M., Aragón-Salamanca A., Frenk C. S., Navarro J. F., Zepf S. E., 1994, *MNRAS*, 271, 781.
- Condon J. J., 1992, *ARA&A*, 30, 575
- Connolly A. J., Szalay A. S., Dickinson M., Subbarao M. U., Brunner R. J., 1997, *ApJ*, 486, L11
- Cowie L. L., Hu E. M., Songaila A., 1995, *Nat*, 377, 603
- Cowie L. L., Songaila A., Barger A. J., 1999, *ApJ*, in press (astro-ph/9904345)
- Cram L. E., 1998, *ApJ*, 508, L85
- Downes D., Solomon P., 1998, *ApJ*, 507, 615
- Dwek E. et al., 1998, *ApJ*, 508, 106
- Dwek E., Arendt R., 1998, *ApJ*, 508, L9
- Eales S. A., Edmunds M. G., 1996, *MNRAS*, 280, 1167
- Eales S. A., Lilly S. J., Gear W. K., Dunne L., Bond J. R., Hammer F., Le Fèvre O., Crampton D., 1999, *ApJ*, 515, 518
- Ellis R. S., 1997, *ARA&A*, 35, 389
- Fall S. M., Pei Y. C., 1993, *ApJ*, 402, 479
- Ferguson A. M. N., Gallagher J., Wyse R. F. G., 1998, *AJ*, 116, 673
- Fixsen D. J., Dwek E., Mather J. C., Bennett C. L., Shafer R. A., 1998, *ApJ*, 508, 123
- Flores H. et al. 1999, *ApJ*, 517, 148
- Frayer D. T., Ivison R. J., Scoville N. Z., Yun M. S., Evans A. S., Smail I., Blain A. W., Kneib J.-P., 1998, *ApJ*, 506, L7
- Frayer D. T. et al., 1999, *ApJ*, 514, L13
- Galleo J., Zamorano J., Aragón-Salamanca A., Rego M., 1996, *ApJ*, 459, L43
- Gardner J. P., Sharples R. M., Carrasco B. E., Frenk C. S., 1996, *MNRAS*, 282, L1
- Genzel R. et al., 1998, *ApJ*, 498, 579
- Gibson B. K., Loewenstein M., Mushotzky R. F., 1998, *MNRAS*, 290, 623
- Glazebrook K., Blake C., Economou F., Lilly S., Colless M., 1999, *MNRAS*, 306, 843
- Gnedin N. Y., Ostriker J. P., 1992, *ApJ*, 400, 1
- Goldader J. D., Joseph R. D., Doyon R., Sanders D. B., 1997, *ApJ*, 474, 104
- Gregorich D. T., Neugebauer G., Soifer B. T., Gunn J. E., Hertler T. L., 1995, *AJ*, 110, 259
- Gronwall C., 1999, in Holt S., Smith E. eds, *After the dark ages: when galaxies were young*. Am. Inst. Phys. Press, Woodbury, NY, p. 335
- Guiderdoni B., Bouchet F. R., Puget J.-L., Lagache G., Hivon E., 1997, *Nat*, 390, 257
- Guiderdoni B., Hivon E., Bouchet F. R., Maffei B., 1998, *MNRAS*, 295, 877
- Gunn K. F., Shanks T., 1999, *MNRAS*, submitted
- Hacking P. B., Houck J. R., 1987, *ApJS*, 63, 311
- Hauser M. G. et al., 1998, *ApJ*, 508, 25
- Hogg D. W., Phinney E. S., 1997, *ApJ*, 488, L95
- Holland W. S. et al., 1998, *Nat*, 392, 788
- Holland W. S. et al., 1999, *MNRAS*, 303, 659
- Hudson M. J., Gwyn S. D. J., Dahle H., Kaiser N., 1998, *ApJ*, 503, 531
- Hughes D. et al., 1998, *Nat*, 394, 241
- Ivison R. J., Smail I., Le Borgne J.-F., Blain A. W., Kneib J.-P., Bézecourt J., Kerr T. H., Davies J. K., 1998, *MNRAS*, 298, 583
- Ivison R. J., Smail I., Barger A. J., Kneib J.-P., Blain A. W., Owen F. N., Kerr T. H., Cowie L. L., 1999, *MNRAS*, submitted
- Jameson A., Longair M. S., Blain A. W., in Gibson B. K., Axelrod T. S., Putman M. E. eds., *The third Stromlo symposium: The Galactic Halo*. Astron. Soc. Pacific conf. series. vol. 165, Astron. Soc. Pac., San Francisco, p. 346
- Jameson A., Blain A. W., Longair M. S., 2000, *MNRAS*, submitted
- Kauffmann G., Charlot S., 1998, *MNRAS*, 294, 705
- Kawara K. et al., 1998, *A&A*, 336, L9
- Lagache G., Abergel A., Boulanger F., Desert F.-X., Puget J.-L., 1999, 344, 322
- Lampton M., Bowyer S., Deharveng J. M., 1990, in Bowyer S., Leinert C. eds., *The galactic and extragalactic background radiation*, Proc. IAU 139, Kluwer, p. 449
- Larson R. B., 1998, *MNRAS*, 301, 569
- Lilly S. J., Tresse L., Hammer F., Crampton D., Le Fèvre O., 1995, *ApJ*, 455, 108
- Lilly S. J., Le Fèvre O., Hammer F., Crampton D., 1996, *ApJ*, 460, L1
- Lilly S. J., Eales S. A., Gear W. K. P., Hammer F., Le Fèvre O., Crampton D., Bond J. R., Dunne L., 1999, *ApJ*, 518, 641
- Longair M. S., 1998, *Galaxy formation*. Springer, Berlin
- Lutz D., Spoon H. H. W., Rigopoulou D., Moorwood A. F. M., Genzel R., 1998, *ApJ*, 505, L103
- Madau P., Ferguson H. C., Dickinson M. E., Giavalisco M., Steidel C. C., Fruchter A., 1996, *MNRAS*, 283, 1388
- Metcalfe N., Shanks T., Campos A., Fong R., Gardner J. P., 1996, *Nat*, 294, 147
- Mihos C., 1999, in Tacconi L., Lutz D. eds. *ULIRG 98*, *Ap&SS*, in press (astro-ph/9903115)
- Mihos J. C., Hernquist L., 1996, *ApJ*, 464, 641
- Murthy J., Hall D., Earl M., Henry R. C., Holby J. B., 1999, *ApJ*, in press
- Mushotzky R. F., Loewenstein M., 1997, *ApJ*, 481, L63
- Nota A., Sirianni M., Leitherer C., De Marchi G., Clampin M., 1998, *BAAS*, 192, 84.01
- Oliver S. J., Rowan-Robinson M., Saunders W., 1992, *MNRAS*, 256, 15P
- Oliver S. J., et al. 1997, *MNRAS*, 289, 471
- Partridge R. B., Richards E. A., Fomalont E. B., Kellermann K. I., Windhorst R. A., 1997, *ApJ*, 483, 38
- Pascarelle S. M., Lanzetta K. M., Fernández-Soto A., 1998, *ApJ*, 508, L1
- Peacock J. A., Dodds S. J., 1994, *MNRAS*, 267, 1020
- Pei Y. C., Fall S. M., 1995, *ApJ*, 454, 69
- Pei Y. C., Fall S. M., Hauser M. G., 1999, *ApJ*, in press (astro-ph/9812182)
- Pettini M., Smith L. J., King D. L., Hunstead R. W., 1997, *ApJ*, 486, 665
- Pettini M., Kellogg M., Steidel C. C., Dickinson M., Adelberger K. L., Giavalisco M., 1998a, *ApJ*, 508, 539
- Pettini M., Steidel C. C., Adelberger K. L., Kellogg M., Dickinson M., Giavalisco M., 1998b, in Shull J. M., Woodward C. E., Thronson H. A. eds, *Cosmic Origins: evolution of galaxies, stars, planets and life*. Astr. Soc. Pac., San Francisco, p. 67
- Pozzetti L., Madau P., Zamorani G., Ferguson H., Bruzual A., 1998, *MNRAS*, 298, 1133
- Press W. H., Schechter P., 1974, *ApJ*, 187, 425
- Puget J.-L., Abergel A., Bernard J.-P., Boulanger F., Burton W. B., Désert F.-X., Hartmann D., 1996, *A&A*, 308, L5
- Puget J.-L. et al., 1999, *A&A*, 345, 29
- Rieke G. H., Loken K., Rieke M. J., Tamblyn P., 1993, *ApJ*, 412, 99
- Rowan-Robinson M., Hughes J., Veda K., Walker D. W., 1990, *MNRAS*, 246, 273
- Saunders W., Rowan-Robinson M., Lawrence A., Efstathiou G., Kaiser N., Ellis R. S., Frenk C. S., 1990, *MNRAS*, 242, 318
- Savage B. D., Sembach K. R., 1996, *ARA&A*, 34, 279
- Sawicki M. J., Lin H., Yee H. K. C., 1997, *AJ*, 113, 1
- Schechter P., 1976, *ApJ*, 203, 297

- Schlegel D. J., Finkbeiner D. P., Davis M., 1998, *ApJ*, 500, 525
- Smail I., Ivison R. J., Blain A. W., 1997, *ApJ*, 490, L5
- Smail I., Ivison R. J., Blain A. W., Kneib J.-P., 1998, *ApJ*, 507, L21
- Smail I., Ivison R. J., Kneib J.-P., Cowie L. L., Blain A. W., Barger A. J., Owen F. N., Morrison G., 1999, *MNRAS*, in press (astro-ph/9905246)
- Smail I., Ivison R. J., Owen F. N., Blain A. W., Kneib J.-P., 2000, *ApJ*, in press (astro-ph/9907083)
- Soifer B., Neugebauer G., 1991, *AJ*, 101, 354
- Somerville R. S., Primack J. R., Faber S. M., 1999, *MNRAS*, in press (astro-ph/9806228)
- Soucail G., Kneib J.-P., Bézecourt J., Metcalfe L., Altieri B., Le Borgne J.-F., 1999, *A&A*, 343, L70
- Stanev T., Franceschini A., 1998, *ApJ*, 494, L159
- Steidel C. C., Giavalisco M., Dickinson M., Adelberger K. L., 1996a, *AJ*, 112, 352
- Steidel C. C., Giavalisco M., Dickinson M., Pettini M., Dickinson M., Adelberger K. L., 1996b, *ApJ*, 462, L17
- Steidel C. C., Adelberger K. L., Dickinson M., Giavalisco M., Pettini M., 1999, *ApJ*, 519, 1
- Storrie-Lombardi L. J., McMahon R. G., Irwin M. J., 1996, *MNRAS*, 283, L79
- Szokoly G. P., Subbarao M. U., Connolly A. J., Mobasher B., 1998, *ApJ*, 492, 452
- Tan J. C., Silk J., Balland C., *ApJ*, in press (astro-ph/9904004)
- Toller G., Tanabe H., Weinberg J. L., 1987, *A&A*, 188, 24
- Trentham N., Blain A. W., Goldader J., 1999, *MNRAS*, 305, 61
- Tresse L., Maddox S. J., 1998, *ApJ*, 495, 691
- Treyer M. A., Ellis R. S., Milliard B., Donas J., Bridges T. J., 1998, *MNRAS*, 300, 303
- Wilner D. J., Wright M. C. H., 1997, *ApJ*, 488, L67
- Yan L., McCarthy P. J., Freudling W., Teplitz H. I., Malumuth E. M., Weymann R. J., Malkan M. A., 1999, *ApJ*, 519, L47
- Zepf S. E., Silk J. E., 1996, *ApJ*, 466, 114